arXiv:1603.01938v1 [astro-ph.GA] 7 Mar 2016

Formation, Evolution, and Revolution of Galaxies by SKA: Activities of SKA-Japan Galaxy Evolution Sub-SWG

Tsutomu T. Takeuchi[1], Kana Morokuma-Matsui,[2], Daisuke Iono[2,3], Hiroyuki Hirashita[4], Wei Leong Tee[4,5], Wei-Hao Wang[4], Rieko Momose[2,6,7], on behalf of the SKA-Japan Galaxy Evolution sub-Science Working Group

[1]Division of Particle and Astrophysical Science, Nagoya University, Furo-cho, Chikusa-ku, Nagoya 464–8602, Japan.
[2]National Astronomical Observatory of Japan, Osawa, Mitaka, Tokyo, Japan
[3]SOKENDAI (The Graduate University for Advanced Studies)
[4]Institute of Astronomy and Astrophysics, Academia Sinica, P.O. Box 23-141, Taipei 10617, Taiwan
[5]Department of Physics, National Taiwan University, Taipei 10617, Taiwan
[6]National Tsing Hua University, Hsinchu, 30013, Taiwan
[7]The Institute for Cosmic Ray Research, the University of Tokyo, Japan

*E-mail: takeuchi.tsutomu@g.mbox.nagoya-u.ac.jp, kana.matsui@nao.ac.jp, d.iono@nao.ac.jp, hirashita@asiaa.sinica.edu.tw, momose.rieko@nao.ac.jp

Abstract

Formation and evolution of galaxies have been a central driving force in the studies of galaxies and cosmology. Recent studies provided a global picture of cosmic star formation history. However, what drives the evolution of star formation activities in galaxies has long been a matter of debate. The key factor of the star formation is the transition of hydrogen from atomic to molecular state, since the star formation is associated with the molecular phase. This transition is also strongly coupled with chemical evolution, because dust grains, i.e., tiny solid particles of heavy elements, play a critical role in molecular formation. Therefore, a comprehensive understanding of neutral–molecular gas transition, star formation and chemical enrichment is necessary to clarify the galaxy formation and evolution. Here we present the activity of SKA-JP galaxy evolution sub-science working group (subSWG) Our activity is focused on three epochs: $z \sim 0$, 1, and $z > 3$. At $z \sim 0$, we try to construct a unified picture of atomic and molecular hydrogen through nearby galaxies in terms of metallicity and other various ISM properties. Up to intermediate redshifts $z \sim 1$, we explore scaling relations including gas and star formation properties, like the main sequence and the Kennicutt–Schmidt law of star forming galaxies. To connect the global studies with spatially-resolved investigations, such relations will be plausibly a viable way. For high redshift objects, the absorption lines of HI 21-cm line will be a very promising observable to explore the properties of gas in galaxies. By these studies, we will surely witness a real revolution in the studies of galaxies by SKA.

Key words: Galaxies: evolution — galaxies: formation — stars: formation — ISM: metallicity — ISM: neutral gas — hydrogen

© 2016 Japan SKA Consortium

1 Introduction

Galaxies evolve. This fact has been a driving force of the studies on galaxies from late 70's when the galactic physics started kicking in, until today. However, how galaxeis formed and evolved still remains far from full understanding. The evolution of galaxies is a change of their various complicated physical properties with time. To be precise, there are two different aspects in galaxy evolution: the individual evolution of a certain galaxy, say, a "personal" history of a galaxy, and the statistical evolution of galaxies at a certain cosmic time, or a "social" history of galaxies. We use one of these different aspects depending on the issue we are concerned. From a cosmological point of view, the dark matter interacts gravitationally to form dark halos, and galaxies form and evolve in the halos. In this case, the dynamical properties are most important. However, the most enthusiastically studied subject of galaxy evolution is the evolution of star formation (SF) activities: stars form in a first gas clump, and first generation stars die and expel the first heavy elements in the Universe, and the formation of the next generation stars is accelerated, and so on. The chemical composition of the interstellar medium (ISM) in galaxies changes with time (chemical evolution: Tinsley 1980). In addition to the snapshot of the SF, the accumulated stellar mass became of interest recently. Not only the evolution of galaxies, but also the mass accretion in the form of dwarf galaxies and remnant gas infall from filamentary structures in the Large-Scale Structure in the Universe change the structure of galaxies. Galaxy merging drastically changes the morphology of galaxies, which is also one of the important aspects of galaxy evolution. There often exists a massive black hole at the center of a galaxy. The activity of an active galactic nucleus (AGN) evolves with the change of the accretion rate to the black hole. A mysterious correlation between the masses of the spheroid component and central black hole in galaxies (Magorrian et al. 1998). This suggests a hidden connection of the evolution of black holes and galaxies, known as "the co-evolution".

During the recent decade, multiwavelength deep galaxy surveys brought us a dramatic view of very high-z Universe. They seem to show that the properties of galaxies are mainly determined by their stellar mass and environment, among others. According to the standard cold dark matter (CDM) scenario, the structure formation proceeds hierarchically, i.e., small halos form tend to form early and they merge each other to form larger, heavier objects. Before galaxy formation, baryons are mostly in gas phase. Then, they fall onto the gravitational potential of halos and form dense molecular clouds. This is the first onset of star formation. Dying stars inject metals and dust into the ISM, which accelerate the next star formation. At the same time, they also provide thermal and kinetic energy to the ISM which hamper the cooling of gas. Thus, the star formation is self-regulating, very complicated process determined by the interplay of DM and baryons. Hence, in order to understand the SF, we must observe the neutral gas in galaxies in various environment as a function of the cosmic time, as many as possible.

However, previous studies on galaxy evolution were dominantly focused on the snapshot of the SF activities in galaxies. The star formation rate (SFR) is observationally estimated by various observables related to massive stars [recombination lines of HII regions, non-ionizing ultraviolet (UV) luminosity, dust emission heated by UV from massive stars, polycyclic aromatic hydrocarbon (PAH) band emission, radio continuum, etc.], but all of them can only give the information of the SFR, and nothing about *the transition from gas to stars*, the fundamental key process of the SF. In radio astronomy, in contrast, traditionally the molecular emission lines have been observed to obtain the information of the material to form stars. Combining the SFR and molecular gas mass, we can discuss the gas–star transition. But still the molecular lines can tell us only about gas in molecular form, and if we want to go further to have a global view of the SF, we must observe the neutral gas. Up to now, because of the limitation of the current instruments, the observation of neutral gas was limited to nearby galaxies, and the properties of neutral gas in galaxies have been rarely discussed in the context of galaxy evolution. The advent of the square kilometre array (SKA) will bring the ultimate, revolutionary breakthrough to the studies on galaxy evolution.

This article is organized as follows: in Section 2, we overview the role of atomic hydrogen (HI) in the context of galaxy evolution. We also summarize the SKA-related researches on galaxy evolution in this section. In Section 3, we introduce the activity of the SKA-JP galaxy evolution sub-science WG. Section 4 is devoted to summary.

2 Current Status of the Studies on Galaxy Evolution — Atomic Hydrogen in Galaxies —

2.1 Atomic and molecular hydrogen

Molecular gas is the key ingredient for star formation in galaxies. Roughly 10% of the mass of the interstellar medium is composed of molecular hydrogen (H_2) in the

Milky Way galaxy (Kalberla & Kerp 2009; Nakanishi & Sofue 2016). This subsection describes the processes responsible for the formation and destruction of molecular hydrogen, and the fractional abundance of atomic and molecular hydrogen. While the principle target line for SKA will be atomic hydrogen, both atomic and molecular lines are intimately connected as seen in the following section. Deep understanding of both phases of the ISM is critical.

2.1.1 Formation of molecular hydrogen

The basic formation path of molecular hydrogen in galaxies is the coupled reaction between two hydrogen atoms, which occurs using electrons and protons as a catalyst. This reaction is accompanied by a significant amount of exothermic energy release. Unless this exothermic energy is deposited into some form of energy, the reaction will reverse and molecules will not form. Therefore, a third atomic hydrogen that will collisionaly remove the excess energy is necessary in order to form the hydrogen molecule. This three hydrogen-atom reaction is efficient in very dense ($n_H > 10^8$ cm^{-3}) environments. In the more diffuse galactic ISM ($n_H \sim 10^5$ cm^{-3}), molecular hydrogen forms using interstellar dust as the catalyst (Gould & Salpeter 1963; Hollenbach & Salpeter 1971). It is believed that the excess energy generated from the bonding of the two hydrogen atoms is absorbed by the random motion of the interstellar dust.

2.1.2 Dissociation of molecular hydrogen

Molecular hydrogen can be dissociated and it can result in two atomic hydrogen. There are three mechanism for this dissociation process. First is the photo-dissociation due to UV photons (Lyman-Werner photons) that are emitted from O or B type stars in the range of 11.2 - 13.6 eV. The second process is the photo-dissociation due to cosmic rays that have 1–100 MeV of energy. The third process is the collisional dissociation in high temperature high density regions. However, it is thought that the collisional dissociation process itself has a minor contribution to the dissociation of molecular hydrogen. This is because molecular hydrogen formation occurs more efficiently than dissociation, due to the efficient depositing of thermal energy generated by molecular hydrogen dissociation and cooling by metals in the ISM.

2.1.3 Atomic and molecular hydrogen in galaxies

The fraction between atomic and molecular gas ($f_{\rm mol} = \rho_{\rm H_2}/\rho_{\rm total}$, $\rho_{\rm total} = \rho_{\rm H_2} + \rho_{\rm HI}$) is determined by the balance between formation and dissociation of molecular hydrogen. Elmegreen (1993) proposed a 1-D model in which the $f_{\rm mol}$ is described by the pressure, UV radiation field, and metalicity in the molecular cloud. Krumholz et al. (2008) expanded Elmegreen (1993)'s model using a spherically symmetric multi-dementional model, and added the formation of molecular hydrogen from interstellar dust as a new parameter. These models reproduce the observations of nearby galaxies and our own galaxy (Sofue et al. 1995; Honma et al. 1995; Blitz & Rosolowsky 2004; Leroy et al. 2008).

Observational check of $f_{\rm mol}$ is mainly performed using the ^{12}CO (J=1–0) line (2.6 mm) emission and the H I (21 cm) line emission. The ^{12}CO (J=1–0) line allows us to derive the line strength and the molecular hydrogen surface density via the conversion factor ($X_{\rm CO}$ [cm^{-2}(K km s^{-1})$^{-1}$]), and the H I line allows us to obtain the surface density of atomic hydrogen. The $f_{\rm mol}$ is derived from these surface densities. The $f_{\rm mol}$ is 25–30 % in late type galaxies (Boselli et al. 2002). Furthermore, the radial distribution of the $f_{\rm mol}$ decreases as a function of radius (e.g., Bigiel & Blitz 2012; Tanaka et al. 2014).

We now describe the density that is required for the transition from atomic to molecular gas. According to analytical models, shielding of atomic hydrogen from photodissociation occurs effectively at $\Sigma_{\rm HI} \sim 10$ M$_\odot$ pc^{-2} ($N_{\rm H} \sim 10^{21}$ cm^{-2}) in a spherical molecular cloud with solar metalicity (Krumholz et al. 2009). In galaxy evolution simulations including molecular hydrogen formation and dissociation, almost all of the atomic hydrogen becomes molecular at $N_{\rm H} \sim 10^{21}$ cm^{-2} in galaxies with similar metallicities (e.g., Pelupessy et al. 2006; Gnedin et al. 2009). Observations of late type galaxies with solar metallicities show similar results to these theoretical predictions (e.g., Wong & Blitz 2002; Bigiel et al. 2008).

The required column density for molecular gas formation depends on the metallicity. Gnedin et al. (2009) suggest that the required column density is higher for low metallicity environments. In their simulations, the dust particles required for shielding from photo-dissociation decreases at low metallicity environments. Therefore, the column density required for shielding becomes higher. Similar results are obtained from other theoretical models and observations of nearby galaxies (e.g., Krumholz et al. 2009; McKee & Krumholz 2010; Fumagalli et al. 2010; Wong et al. 2013; Richings et al. 2014), and thus the metallicity appears to be the key parameter that controls the process that converts from atomic to molecular hydrogen.

2.2 Atomic hydrogen in spiral galaxies

Observations of atomic hydrogen gas (H I gas) in spiral galaxies goes back to the 1950's. Ever since, a large number of galaxies have been observed from very nearby (~ 50 kpc) to distances larger than 100 Mpc ($z > 0.024$), using single dish and interferometers. A summary of the physical understanding of atomic gas in galaxies obtained through H I observations in spiral galaxies is presented in this subsection.

2.2.1 Spatial distribution

There are three major characteristics in the distribution of H I in spiral galaxies. First is the decrease in the galactic center, where the density of the ISM is high. Therefore, most of the hydrogen is in molecular form, and the abundance of H I gas is very low.

The second characteristic is that the H I gas is more extended than the optical disk (e.g., Sancisi 1983; Leroy et al. 2008)). As such, H I gas is often 2-3 times more extended than disk stars in many of the spiral galaxies (e.g., Sancisi 1983). The H I gas seen in the outskirts of spiral galaxies are called circum-galactic medium (CGM). Theoretically, the CGM is thought to be related to large scale gas accretion or gas outflow (e.g., Mori et al. 2002; Mori & Umemura 2006; Dekel et al. 2009a, 2009b; Scannapieco et al. 2005), and they are intimately connected to the mass accretion process and star formation history in galaxies. It is difficult to directly detect the gas in the CGM, mainly because the column density of H I gas in the CGM is lower than the disk gas ($N_{\rm HI} < 10^{19}$ cm^{-2}). However, the advancement in recent receivers have allowed deep and sensitive H I observations, and the diffuse H I gas ($N_{\rm HI} \sim 10^{18}$ cm^{-2}) in the CGM has been detected (Wolfe et al. 2013; Pisano 2014). Possibility of gas inflow onto spiral galaxies have been proposed based on these new data.

The third characteristics is that the surface density ($\Sigma_{\rm HI}$ [M$_\odot$ pc^{-2}]) of H I in the exterior of spiral galaxies are fairly constant and decreases at the exterior. The $\Sigma_{\rm HI}$ is low at the center, and increases as a function of radius, peaking at some radius ($\Sigma_{\rm HI}^{\rm max}$). The $\Sigma_{\rm HI}$ beyond this peak radius is fairly flat and constant (e.g., Sofue & Rubin 2001; Leroy et al. 2008; Bigiel & Blitz 2012). $\Sigma_{\rm HI}^{\rm max}$ only goes as high as ~ 10 M$_\odot$ pc^{-2} because atomic hydrogen becomes molecular when $\Sigma_{\rm HI}^{\rm max} > 10$ M$_\odot$ pc^{-2}.

2.2.2 H I gas mass

The observed H I gas mass in spiral galaxies is M$_{\rm HI} \sim 10^{8-10}$ M$_\odot$ (Walter et al. 2008). In particular, sources with M$_{\rm HI} \sim 10^{10}$ M$_\odot$ are often colliding galaxies, and therefore galaxy interaction can bring significant amount of material into the galaxy.

It is known that the total H I mass and the disk size in spiral galaxies show a correlation. As described in §4.3.2, $\Sigma_{\rm HI}$ in the exteriors of spiral galaxies is almost constant. If we assume that $\Sigma_{\rm HI}$ is constant across the galaxy disk, then the total H I mass of a spiral galaxy is roughly proportional to the area of the galaxy. In fact, it is suggested from observations that the total H I mass correlates with the radius of the stellar disk (e.g., Bigiel & Blitz 2012)).

2.2.3 Kinematical information

One can determine the mass distribution of the galaxy from the kinematical information provided by HI observations. While the rotation velocity varies from 150 - 300 km s^{-1} on average, the basic characteristic is that the rotation increases as a function of radius until some radius, beyond which the velocity is nearly constant ($v_{\rm max}$) (e.g., Rubin et al. 1980, 1985; Bosma et al. 1981; Sancisi & van Albada 1987a, 1987b), due to dark matter.

2.2.4 Tully–Fisher relation

The rotation velocity and the brightness of spiral galaxies are correlated, in what is called the Tully-Fisher relation (Tully & Fisher 1977, TF relation:). It is known that the scatter in the TF relation is larger at the low mass end. This is due to the fact that the fraction of gas mass becomes non-negligible for low mass spiral galaxies. The correlation becomes tighter when the total baryon mass ($M_{\rm baryon} = M_{\rm star} + M_{\rm gas}$) is used instead of the stellar mass (e.g., Bell & de Jong 2001). This is called the baryon-Tully-Fisher relation (BTF relation). Observational confirmation of the BTF relation is currently ongoing, using the recent gas survey observations of spiral galaxies (e.g., McGaugh 2012).

The TF relation is used to measure the distance to spiral galaxies. The true brightness of the galaxy can be estimated from the TF relation and the H I rotation curve. On the other hand, the apparent brightness of the galaxy depends on the distance. Therefore, the difference between the apparent and the true brightnesses allows us to determine the distance to the spiral galaxy. Up to now, the H I velocity and the stellar spectroscopy were used to estimate the distances. More recently, the BTF relation has been used to get an accurate measure of the distances (e.g., Bell & de Jong 2001). However, significant uncertainties are present in the derivation of the stellar and gas masses, and therefore uncertainties in the derived distances (e.g., Zaritsky et al. 2014).

2.3 Atomic hydrogen in early-type galaxies

Early type galaxies (ETGs, elliptical and lenticular galaxies) have been considered to be characterized by higher bulge-to-disk ratio and older stellar population compared to late type galaxies (LTGs, spiral galaxies). Recent observations revealed the variety of ETGs in morphology, e.g. existence of ETGs with bulge-to-disk ratio comparable to LTGs (Spitzer & Baade 1951; Sandage et al. 1970; van den Bergh 1976), as well as in star formation activity (e.g., Kuntschner et al. 2010). In this section, we take a look back to simple histories of H I observations targeting ETGs and introduce some science outputs from ATLAS^{3D}, one of the largest surveys toward ETGs.

2.3.1 Single-dish studies

ETGs have been observed in H I since 1960 era. Although interferometric observation can achieve higher angular resolution than single-dish observation, single-dish H I observations enable us to measure total amount of atomic gas and line-width of galactic H I spectra without so-called "missing-flux" problem (interferometer does not have a sensitivity on extended structure). In 1960s, H I observations of ETGs revealed that the ratios of H I mass to B-band luminosity of ETGs are lower than those of LTGs (e.g., Gouguenheim et al. 1969). Based on these observations, H I gas masses of 15 % of ~ 150 ellipticals and 25 % of ~ 300 lenticulars were successfully measured with a typical detection mass limit of a few times 10^8 $M_\odot$ (Knapp et al. 1985; Wardle & Knapp 1986).

In 2000s and beyond, H I blind surveys, such as HIPASS (Barnes et al. 2001) and ALFALFA (Giovanelli et al. 2005) have revealed a strong environmental dependence of H I detection rate: a few % in the galaxy cluster environment whereas 40 % in the field environment (di Serego et al. 2007; Grossi et al. 2009). These results are consistent with the idea of Giovanelli & Haynes (1983) that H I gas is easily stripped from galaxies in cluster environment as well as the other recent observations showing that star-forming ETGs reside in low galaxy density region (Thomas et al. 2010).

2.3.2 Interferometric studies

In 1980s, detailed spatial distribution of H I gas in ETGs have been investigated using interferometric data. Despite the appearance in optical images, ETGs show a wide variety of H I spatial distribution, such as large disk extending to tens of kpc, low-density disk, ring structure, and unsettled gas distributions indicating recent gas accretion, gas stripping, galaxy interaction and merging (van Gorkom & Schiminovich 1997; Hibbard et al. 2001, and reference therein). These study revealed that H I gas is one of the ideal tracers of recent mass assembly history of ETGs.

With Westerbork Synthesis Radio Telescope (WSRT), Morganti et al. (2006) and Oosterloo et al. (2010) conducted deep H I imaging observations of 33 ETGs selected from SAURON project[1], which is deep enough to detect H I mass down to $\sim (2-3) \times 10^6$ $M_\odot$. They confirmed environmental dependence of H I detection rate, where H I emissions are detected from 10 % and 2/3 of all ETGs inside and outside the Virgo cluster, respectively. They revealed that the faintest signature of H I accretion is presented in most H I-detected ETGs. In addition, they find that all ETGs with a settled H I distribution host ionized and molecular gas, suggesting recent star formation.

2.3.3 H I survey towards ATLAS^{3D} galaxies

Serra et al. (2012) observed 170 ETGs in H I with WSRT as a part of ATLAS^{3D} project. The ATLAS^{3D} project combines multi-wavelength surveys specialized in ETGs (Cappellari et al. 2011). This project targets a complete sample of 260 early-type galaxies with K-band absolute magnitude of brighter than -21.5 within the local Universe (42 Mpc). The achieved H I mass sensitivity is down to $(5-50) \times 10^6$ $M_\odot$ and H I emissions were detected from 53 ETGs. Based on this data, they revealed the properties of H I gas in ETGs as follows:

- A wide variety of H I morphology: H I-detected ETGs shows disk and ring structures (~ 64 %), unsettled structure including a tail structure which is indicative of tidal effect or gas accretion (~ 26 %), and clumpy structure distributed over the entire galaxy (~ 9 %). ETGs with extended H I disk ($> 3.5 \times R_e$) have large amount of H I gas (5×10^9 $M_\odot$) and different kinematics to stellar component, whereas ETGs with small H I disk have small amount of H I gas ($< 10^8$ $M_\odot$) and the same kinematics with stellar component.
- Signature of star formation: 70 % of ETGs with H I gas within $\sim 1R_e$ region show star formation activity, and their central regions are dominated by molecular gas.
- H I mass function: The characteristic mass is $\sim 2 \times 10^9$ $M_\odot$ and the slope at lower mass is -0.7, when the H I mass function is fitted with a Schechter function.
- Comparison with LTGs: H I mass of ETGs is mostly lower than that of LTGs but some ETGs have H I mass comparable to that of LTGs. The high-H I-column-density component observed in bright stellar disk of

[1] SAURON (Spectroscopic Areal Unit for Research on Optical Nebulae) is a name of the panoramic integral field spectrograph as well as a name of the scientific project whose main goal is to understand the formation and evolution of elliptical and lenticular galaxies and of spiral bulges from 3D observations (Bacon et al. 2001).

LTGs is not seen in ETGs.

- Environmental effect on the nature of ETGs: The environmental effect on H I gas mass in ETGs was confirmed, where cluster ETGs tend to have lower detection rate of H I emission (~ 10 %) compared to field ETGs (~ 40 %). The H I gas mass and $M_{\rm HI}/L_K$ decrease as the number density of galaxies increases.
  In addition, H I morphology correlate with the number density of galaxies, where ETGs with larger H I disk and ring structures tend to reside in lower galaxy density and ETGs with unsettled H I structure tend to reside in typical galaxy density of rich group. This results indicate that processes working in galaxy-cluster scale are important for ETG evolution.

2.4 Atomic hydrogen in dwarf galaxies

Understanding star formation in dwarf galaxies is important step for understanding star formation in early Universe. Dwarf galaxies are considered to reside in low-mass dark matter halos (DHs), and that the first star has been formed in such low mass DHs in ΛCDM model (Yoshida et al. 2006, 2008). In addition, revealing the nature of dwarf galaxies is also important for galaxy evolution since dwarf galaxies are considered to be a building block of larger galaxies.

Large galaxy surveys have been conducted mainly in optical and near infrared wavelengths, while these surveys tends to be biased to relatively bright and massive galaxies. Recent H I galaxy surveys, on the other hand, have discovered a lot of gas-rich dwarf galaxies. In this section, H I surveys specialized in dwarf galaxies are introduced.

2.4.1 H I survey toward dwarf galaxies

In the past 10 years, detailed kinematics and stellar population of dwarf galaxies with H I mass of $> 10^8$ $M_\odot$ have been investigated. ALFALFA (Arecibo Legacy Fast ALFA Survey, Giovanelli et al. 2005), which is a large and unbiased H I survey, discovered a few times 100 dwarf galaxies with H I mass $< 10^8$ $M_\odot$, and provided us a statistically reliable H I mass function of galaxies for the first time (Martin et al. 2010). In the following paragraphs, four representative H I surveys towards dwarf galaxies with lower H I gas mass are introduced.

The FIGGS (Faint Irregular Galaxies GMRT Survey, Begum et al. 2008), LITTLE THINGS (Local Irregulars That Trace Luminosity Extremes, The H I Nearby Galaxy Survey, Hunter et al. 2012), and VLA-ANGST (VLA A High-resolution H I Survey of Nearby Dwarf Galaxies, Ott et al. 2012) target dwarf galaxies with relatively small H I mass, 8.5×10^7, 2.7×10^7 and 2.3×10^7 $M_\odot$ as a median value, respectively. 21 dwarf galaxies with H I mass of $< 10^7$ $M_\odot$ were also observed in those surveys (5, LITTLE THINGS; 7, FIGSS; 9, VLA-ANGST). SHIELD (Survey of H I in Extremely Low-mass Dwarfs, Cannon et al. 2011) targets dwarf galaxies with $10^6 - 10^7$ $M_\odot$. The scientific meanings of studying H I gas in dwarfs are as follows:

- Gas-rich dwarf galaxies: H I surveys toward dwarf galaxies revealed the existence of gas-rich systems (Begum et al. 2008; Hunter et al. 2012; Ott et al. 2012). The existence of such gas-rich galaxies with very shallow potential wells poses interesting puzzles for the ΛCDM paradigm. This is because that cold gas in shallow potential wells is expected to be easily striped by ram pressure (e.g., Lewis et al. 2002; Grebel et al. 2003), be blown out by star formation activity (e.g., Mac Low & Ferrara 1999; Ferrara & Tolstoy 2000), and be vaporized by hot intergalactic medium (Benson et al. 2002). In addition, the UV radiation field inhibits gas accretion and cooling in low-mass halos (Rees 1986; Babul & Rees 1992; Benson et al. 2002; Hoeft et al. 2006). Studying such gas-rich dwarfs lead to the understanding of the gas deficiency processes of galaxies described above.
- Star formation under the extreme environment: Star formation is often induced by gas compression due to external perturbations such as galactic shock at the spiral arms in disk galaxies and galaxy mergers. Dwarf galaxy is a suitable object to study star formation without these external perturbations.
- Baryonic Tully-Fisher relation: Dwarf galaxies do not follow the same Tully-Fisher relation of spiral galaxies. However, once the baryon mass is used instead of galaxy luminosity, i.e., baryonic Tully-FIsher relation, they follow the same relation (McGaugh et al. 2000, 2005), suggesting a close link between dark matter halo and baryonic components of galaxies. Studying baryonic Tully-Fisher relation leads to the understanding of the relationship between evolutions of dark matter and baryonic components of galaxies.
- Dark matter profile: Dwarf galaxies are suitable targets to study the density profile of dark matter halos. Cosmological simulations of hierarchical galaxy formation predict a "universal" cusped density core for the dark matter haloes of galaxies (e.g., Navarro et al. 2004). Although some observation support the theoretical prediction (e.g., van den Bosch & Swaters 2001; de Blok et al. 2005), other observations indicate a constant-density core for their dark matter haloes (e.g., de Blok et al. 2003; Weldrake et al. 2003). This is a

so-called "core-cusp problem". Dark matter profiles estimated by observations generally contain a significant error originated in the estimation of M/L. However, it is possible to estimate dark matter profile of dwarf galaxy with a small contribution from stellar component.

2.5 H I surveys covering various population of galaxies

Investigating statistical properties of galaxies is also important for understanding galaxy evolution as well as detailed studies on individual galaxies. In the previous subsections, we focused on the H I studies on spiral (sec. 2.2), early-type (sec. 2.3) and dwarf galaxies (sec. 2.4). In this subsection, we first introduce one of the largest H I survey of local galaxies, GASS project, and then two pioneering H I surveys targeting galaxies in the ranges of $0.1 < z < 1$, BUDHIES and CHILES projects.

2.5.1 GALEX Arecibo SDSS Survey (GASS)

The bimodal distribution of galaxies in stellar mass versus $u-r$ color plot ("galaxy bimodality", Struve & Conway 2012) is one of the important scientific output from large galaxy surveys in optical wavelength, such as SDSS (Sloan Digital Sky Survey, York et al. 2000): "blue clouds" galaxies which are actively forming stars ($< 3 \times 10^{10}$ M$_\odot$); "red sequence" galaxies which are not currently forming stars ($> 3 \times 10^{10}$ M$_\odot$). Galaxies distributed between the two sequences are referred to as "green valley" galaxies.

GALEX Arecibo SDSS Survey (GASS) is an H I survey specifically designed to measure H I mass of ~ 1000 galaxies in the local Universe ($0.025 < z < 0.05$) with stellar masses $10^{10} < M_\star < 10^{11.5}$ M$_\odot$. The stellar mass range is determined to straddles the "transition mass" of 3×10^{10} M$_\odot$ between blue cloud and red sequence galaxies. This is because that one of the main goal of GASS project is to identify and quantify the incidence of galaxies that are transitioning between the blue, star-forming cloud and the red sequence of passively evolving galaxies ("transition galaxies"). Here, main seven scientific outputs of the project are introduced:

- H I gas mass fraction (Cantinella et al. 2010, 2012a): Cantinella et al. suggested that candidates of "transition galaxies" can be identified as outliers from the mean scaling relations between H I gas mass fraction ($M_{\rm HI}/M_\star$, where $M_{\rm HI}$ is H I gas mass) and other galaxy properties. They found a scaling relation of galaxies among H I gas mass $M_{\rm HI}$, surface density of stellar mass $\mu_\star$, and $NUV-r$ color and interesting outliers from this plane: gas-rich red sequence galaxies that may be in the process of regrowing their discs, as well as blue, but gas-poor spirals.
- Star formation efficiency (Schiminovich et al. 2010): Schiminovich et al. suggested candidates of "transition galaxies" are identified as (1) H I-rich but low-SFR and (2) H I-poor but high-SFR galaxies. They explored the global scaling relations associated with the bin-averaged ratio of the SFR over the H I mass (i.e. $\Sigma_{\rm SFR}/\Sigma_{M_{\rm HI}}$), which is the H I-based star formation efficiency (SFE). They found that the H I-based SFE remains relatively constant across the sample with a value of $10^{-9.5}$ yr^{-1} (or an equivalent gas consumption time-scale of $\sim 3 \times 10^9$ yr) while 10 % of galaxies have higher or lower SFE than the average value. Such outliers are expected to have potential for a change (either decrease or increase) in their sSFR in the near future.
- Inside-out formation of Galactic discs (Wang et al. 2011): Wang et al. found an observational evidence indicating "inside-out" formation of galactic disks. They showed that galaxies with larger H I fraction have bluer, more actively star-forming outer disks compared to the inner part of the galaxy. They also found H I fraction and galaxy asymmetry do not have intrinsic connection, which suggests that gas is accreted smoothly on to the outer disc.
- Baryonic mass-velocity-size relations (Cantinella et al. 2012b): Cantinella et al. found a generalized baryonic Faber-Jackson (BFJ) relation that holds for all the galaxies in their sample, regardless of morphology, inclination or gas content, and has a scatter smaller than 0.1 dex. They compared baryonic Tully-Fisher (BTF) and BFJ relations for GASS sample, and investigated how galaxies scatter around the best fits obtained for subsets of disk-dominated and bulge-dominated systems. They demonstrated that by applying a simple correction to the stellar velocity dispersions that depends only on the concentration index of the galaxy, disks and spheroids distribute on to the same dynamical relation. This generalized BFJ relation indicates that there is a fundamental correlation between the global dark matter and baryonic content of galaxies regardless of morphology.
- H I content and metal enrichment at galactic outskirts (Moran et al. 2012): Moran et al. found that H I-rich galaxies tend to have larger metallicity drops in their outer disks, suggesting the accretion or radial transport of relatively pristine gas from beyond the galaxies' stellar disks. They investigated radial metallicity profile of 174 star-forming galaxies using long-slit spectra and found that ~ 10 % of their sample exhibit a sharp downturn in metallicity. They also found that

the magnitude of the outer metallicity drop is well correlated with the total H I content of the galaxy.

- Bivariate neutral hydrogen-stellar mass function (Lemonias et al. 2013): Lemonias et al. investigated the bivariate neutral atomic hydrogen (H I)-stellar mass function (HISMF) $\phi(M_{\rm HI}, M_\star)$ for 480 GASS galaxies. Based on the fitting to HISMF with Schechter function, they found that the slope of the HISMF at moderate H I masses correlate with stellar mass and SFR, whereas the characteristic H I mass varies weakly with them.
- Environmental effect (Cantinella et al. 2013): Cantinella et al. claimed the importance of stripping of the cold interstellar medium in galaxy groups for galaxy evolution, which has not been considered in semi-analytic models of galaxy formation. They found that massive galaxies located in haloes with masses of $10^{13} - 10^{14}$ $M_\odot$ have at least 0.4 dex less H I than objects in lower density environments.

2.5.2 Blind Ultra Deep H I Survey (Verheijen et al. 2007, BUDHIES,)

BUDHIES is a deep H I survey of galaxies in two clusters in intermediate redshifts, Abell 2192 ($z = 0.187$) and Abell 963 ($z = 0.206$), and the large-scale structure of the Universe around them with WSRT. Abell 963 is a massive lensing Butcher-Oemler (Butcher & Oemler 1978) cluster with a large fraction of blue galaxies ($f_{\rm B} = 0.19$, Butcher et al. 1983), and a total X-ray luminosity of $L_X \simeq 3.4 \pm 1 \times 10^{44} h^{-2}$ erg s^{-1} (Allen et al. 2003). Abell 2192 is a less massive cluster in the process of forming, with a high degree of substructure (Jaffé et al. 2012). This cluster is barely detected in X-rays ($L_X \simeq 7 \times 10^{43} h^{-2}$ erg s^{-1}; Voges et al. 1999).

The survey aims at understanding where, how, and why star-forming spiral galaxies get transformed into passive early-type galaxies. In this project, H I emissions were successfully detected in 127 galaxies of Abell 963 and 36 of Abell 2192 with H I masses of 2×10^9 $M_\odot$. In Abell 2192, Jaffé et al. found that the incidence of H I-detections significantly correlates with environment (Jaffé et al. 2012, 2013): at large clustercentric radii ($> 2 - 3$ virial radii), many galaxies are detected in H I, while at the core of the forming cluster, none of the galaxies are H I-detected. They found that this effect starts to become significant in low-mass groups that pre-process the galaxies before they enter the cluster, so that by the time the group galaxies fall into the cluster they may already be H I deficient or even devoid of H I.

2.5.3 COSMOS H I Large Extragalactic Survey (CHILES, Fernández et al. 2013)

CHILES is a 1000-hrs Very Large Array (VLA) project to produce the first H I deep field. The observations are carried out with the VLA in B configuration and cover a redshift range of $0 < z < 0.45$. The field is centered at the COSMOS field (Cosmic Evolution Survey, Scoville et al. 2007), which has been already observed in from radio to X-ray. This project will provide H I images of at least 300 galaxies spread over the entire redshift range to investigate the following topics: 1) H I content, morphology and kinematics of individual galaxies, 2) H I mass function, 3) Cosmic Neutral Gas Density, 4) Environmental suppression of star formation, and 5) Dark haloes and baryons. Fernández et al. (2013) presented initial results based on 50-hrs observations. They detected H I emissions from 33 galaxies within $34' \times 34'$ field for now, including three without a previously known spectroscopic redshift. The highest redshift of galaxies with H I measurement is $z = 0.176$.

2.6 Toward higher-redshifts: revealing galaxy evolution through H I absorption line systems

In observing distant galaxies, because of limited sensitivities of observational facilities, the sample is always biased to the brightest populations. Moreover, since the emission from a galaxy is often related to its star formation activity, it is relatively easy to detect a growing galaxy population whose star formation rate is high or a grown galaxy population which has already built up its stellar mass. This means that the observations of the emission from distant or high-redshift (high-z) galaxies tend to miss ones which have not yet converted a significant fraction of the ISM to stars.

Such galaxies with gas-rich and low-stellar-mass properties can be sampled if we directly sample galaxies with its gas content. The most common method of sampling this kind of galaxies is to observe gas absorption lines in bright continuum spectra of background quasars [quasi-stellar objects (QSOs)]. In particular, Lyα absorption in the continuum spectra of QSOs is useful to identify the foreground (intervening) neutral hydrogen (H I) in the ISM and the intergalactic medium (IGM) over a wide column density range. A sample taken by this method is called Lyα absorption-line systems or Lyα forest (Sargent et al. 1980; Smith et al. 1986; Wolfe et al. 1986).

Damped Lyman α systems (DLAs) are the QSO absorption-line systems whose H I column density is higher than 2×10^{20} cm^{-2} (Prochaska & Wolfe 2000). Because of the prominent Lyα absorption in bright QSO

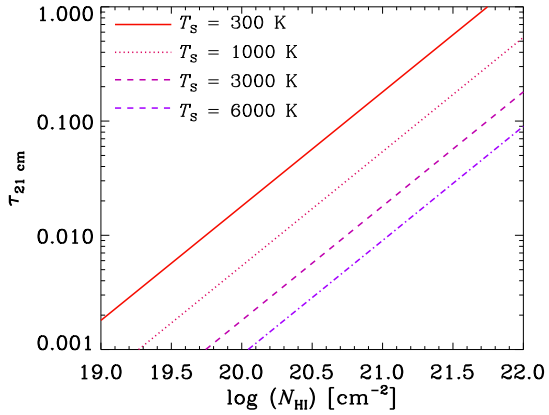


Fig. 1. H I 21 cm absorption optical depth $\tau_{21\,\mathrm{cm}}$ as a function of H I column density N_{HI} with various spin temperatures ($T_{\mathrm{s}} = 300$, 1,000, 3,000, and 6,000 K for the solid, dotted, dashed, and dot-dashed lines, respectively). The velocity dispersion is fixed as $\Delta v = 10$ km s^{-1}.

continuum, DLAs provide us with unique opportunities to trace high-z galaxy evolution. The statistics of H I column density in DLAs is expected to reflect the total H I abundance contained in high-z objects (Péroux et al. 2003) and the density structure of the interstellar medium (ISM) in them (Razoumov et al. 2006).

The hyperfine transition of H I at a wavelength of 21 cm is also known to be a good tracer of H I. While the Lyα absorption is determined by the H I column density, N_{HI}, along the line of sight, the 21 cm optical depth, $\tau_{21\,\mathrm{cm}}$, depends on the spin temperature as well (e.g., Furlanetto et al. 2006):

$$\tau_{21\,\mathrm{cm}} = 0.054 \left(\frac{T_{\mathrm{s}}}{10^3\,\mathrm{K}}\right)^{-1} \left(\frac{\Delta v}{10\,\mathrm{km\,s^{-1}}}\right)^{-1} \left(\frac{N_{\mathrm{HI}}}{10^{21}\,\mathrm{cm^{-2}}}\right), \quad (1)$$

where T_{s} is the spin temperature of hydrogen atoms and Δv is the velocity dispersion. Therefore, combination of Lyα and 21 cm optical depths enables us to derive both column density and temperature. In Figure 1, we show $\tau_{21\,\mathrm{cm}}$ as a function of N_{HI} for various T_{s} with $\Delta v = 10$ km s^{-1}.

There have been some attempts to detect 21 cm line absorption in the radio continuum of DLA-bearing quasars. The fraction of DLAs with detection of 21 cm absorption is, however, low (e.g. Curran et al. 2010). A systematic 21 cm absorption surveys of DLAs has been carried out by Srianand et al. (2012) using the Giant Metrewave Radio Telescope (GMRT) and the Green Bank Telescope (GBT), but 21 cm absorption is detected for only one out of ten DLAs at $2 < z_{\mathrm{abs}} < 3.4$ (z_{abs} is the absorption redshift of the DLA). They further included samples in the literature, and interpreted the small fraction of 21 cm absorption detection as a large covering fraction of the warm neutral medium with temperature $\gtrsim 10^3$ K in the DLA host galaxies (see also Kanekar et al. 2013, 2014). Even for the detected cases, the derived spin temperatures are mostly high ($\sim 10^3$ K) (see also Wolfe & Davis 1979; Wolfe et al. 1985; de Bruyn, O'Dea, & Baum 1996; Carilli et al. 1996; Briggs, Brinks, & Wolfe 1997; Kanekar et al. 2006).

It has been pointed out that DLAs may be biased to systems with low dust extinction: if a foreground system has high dust extinction, the ultraviolet (UV) continuum of the background QSO can become too faint to be detected by optical telescopes (Fall & Pei 1993). The detection rate of high-N_{HI} DLAs may be significantly suppressed by dust extinction (Vladilo & Péroux 2005). This bias could be avoided if we sample background QSOs at radio frequencies, where the effect of dust extinction is negligible. In fact, systematic studies of DLAs for radio-selected QSOs have been performed (e.g., Akerman et al. 2005; Ellison et al. 2005). Although these samples did not show the presence of a significant bias caused by dust extinction, the sample size is not large enough. In particular, the number of systems rapidly declines as N_{HI} becomes large. Sampling of a large number of QSO in the radio will be one of the most important goal of SKA surveys in the future. With a large-area (∼10,000 deg^2) survey with SKA1-MID proposed by Morganti et al. (2015), 5σ detection of typical DLAs with $\tau_{21\,\mathrm{cm}} \sim 0.015$ would be possible against background sources > 30 mJy ($\tau_{21\,\mathrm{cm}} \sim 0.05$ against ∼10 mJy and $\tau_{21\,\mathrm{cm}} \sim 0.1$ against ∼2–3 mJy) up to $z \sim 3$, which is limited by the lowest frequency of SKA-MID (350 MHz). Surveys with SKA1-LOW would extend the redshift range towards higher z.

Before SKA, the following pathfinder observations are planned (Morganti et al. 2015). The Australian Square Kilometre Array Pathfinder (ASKAP) has a wide field of view (FoV ~ 30 deg^2) and frequency coverage down to 700 MHz. The ASKAP First Large Absorption Survey in H I (FLASH) will be able to detect bright QSOs and radio galaxies, and will open up systematic studies of intervening 21 cm absorption at $0.5 < z < 1$. With the planned integration time of 2 hours per field, the 5 σ detection limit for the 21 cm absorption optical depth is $\tau_{21\,\mathrm{cm}} \sim 0.01$ for 1 Jy background sources while it is $\tau_{21\,\mathrm{cm}} \sim 0.3$ for 50 mJy sources. Apertif and MeerKAT will achieve deeper $\tau_{21\,\mathrm{cm}}$ limits with smaller survey areas.

2.7 Galaxy evolution history through radio continuum

Radio continuum emission from galaxies is composed of thermal free–free radiation from H II regions and non-thermal synchrotron radiation from supernova remnants (Condon 1992) (for the simplicity of discussion, we do not consider radio emission from AGNs in this section). Since both of these emission sources are related to massive stars, the luminosity of radio continuum is known to be a good indicator of star formation rate (Condon 1992). Unlike UV–optical star formation indicators, radio continuum is not affected by dust extinction, so that no correction for dust extinction is required in the conversion from radio continuum luminosity to star formation rate. If we detect radio continuum emission from galaxies up to high redshifts, we can in principle clarify the cosmic star formation history.

Another extinction-free star formation indicator is far-infrared (FIR) continuum luminosity (Kennicutt 1998; Inoue et al. 2000). It is known that radio and FIR continuum luminosities are tightly correlated (Condon 1992; Yun et al. 2001). This radio–FIR correlation holds very well for nearby star-forming galaxies. However, whether or not galaxies keep the radio–FIR correlation over their evolution is not obvious. It is rather expected that the radio–FIR relation changes as galaxies evolve, since FIR emission depends on the dust content and radio emission is affected by interstellar magnetic field strength and production/diffusion of high-energy electrons. The different time-scales of these processes may indicate a possibility that the radio–FIR relation changes at high redshifts. It has been clarified observationally that the radio–FIR hold with a factor of 2–3 times smaller FIR/radio ratio at $z \lesssim 2$ (e.g., Garrett 2002; Gruppioni et al. 2003; Ibar et al. 2008; Murphy 2009). Michałowski et al. (2010) reported a similar relation to $z \sim 2$ holds even at $z \sim 5$.

The understanding of dust emission in high-redshift galaxies is rapidly progressing because of advanced observational facilities such as *Herschel* (e.g., Rowlands et al. 2014). ALMA, with its unprecedented sensitivity, is starting to reveal the high-redshift star formation activities through dust emission. However, the narrow FoV of ALMA makes the survey efficiency low. At radio wavelengths, on the other hand, although some surveys are planned using the Jansky Very Large Array (JVLA), future SKA observations are crucial to detect "normal" star-forming galaxies whose star formation rate is ~ 10 $M_\odot$ yr^{-1} (Murphy 2009; Jarvis et al. 2015). The wide FoV of SKA will provide a unique opportunity of tracing the cosmic star formation history at wavelengths free from dust extinction.

Murphy et al. (2015) focused on the ultra-deep SKA1-MID/Band 5 reference survey (Prandoni & Seymour 2015) at a frequency range of 4.6–13.8 GHz. Most previous surveys targeted low frequencies such as 1.4 GHz because FoVs are wider and galaxies are brighter. For example, Seymour et al. (2008) derived the cosmic star formation history at $z < 3$ using Multi-Element Radio-LInked Network (MERLIN) and the Very Large Array (VLA) at 1.4 GHz as well as the VLA at 4.8 GHz, obtaining a consistent star formation history with various optical surveys (see also Morrison et al. 2010). Smolčić et al. (2009) derived the cosmic star formation history and the evolution of radio luminosity function out to $z = 1.3$ by observing the COSMOS field with the VLA at 1.4 GHz. Smolčić et al. (2014) observed the same field at an even lower frequencies (324 MHz) by the VLA, and found objects with steep spectral slopes at $z \gtrsim 1$.

Compared to those surveys, Murphy et al. (2015) focus on higher frequencies for SKA, since the high sensitivity of SKA enables us to perform a survey deep enough even at frequencies $\gtrsim 10$ GHz. According to their expectation, about 30 and 85 sources per arcmin^2 are detected. Such a high frequency has an advantage of high angular resolution. If we can take a 200 km baseline, an angular resolution of < 0.03 arcsec can be achieved at >10 GHz (yet with enough short-baseline data to prevent galaxies from being resolved out), which means that we can resolve 250 pc at $z \gtrsim 1$. This angular resolution matches what is achieved by future space optical–near-infrared telescopes such as *James Webb Space Telescope* (*JWST*)[2]. Another advantage of high-frequency surveys is that the contribution from free–free emission is relatively large compared to low frequencies (such as 1.4 GHz). At high redshift, it is expected that high-energy electrons lose their energy through inverse Compton scattering of the cosmic background radiation, which means that synchrotron emission may not be a good indicator of the star formation activities at high redshift (Murphy 2009).

It is worth mentioning the comparison with Next Generation Very Large Array (ngVLA) (Casey et al. 2015). The ngVLA will achieve a factor of 5–10 times improvement over the current JVLA. By assuming 10 times better sensitivity than VLA, ngVLA it will achieve a 5σ detection limit of 0.06 μJy for 1000 hr of integration time (we multiplied 0.1 to the detection limit estimated for JVLA by Murphy et al. 2015) at 10 GHz. As cited in Section 3.4.2, SKA1-MID and SKA2-MID will achieve a 5 σ detection limit of 0.2 and 0.02 μJy, respectively, with 1000 hr of integration . Therefore, ngVLA will have an intermediate capability between SKA1-MID and SKA2-MID. For convenience, we show the detection limit at

[2] http://www.jwst.nasa.gov/

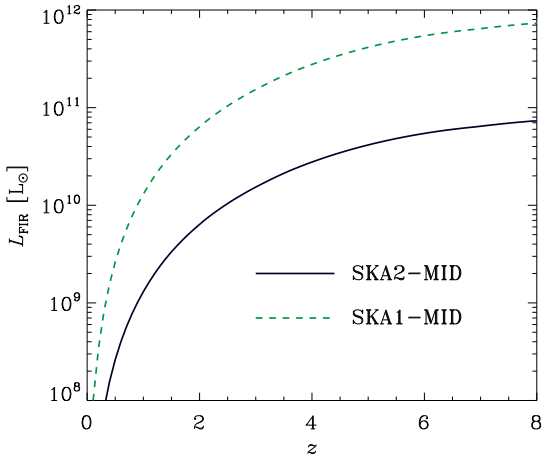


Fig. 2. The total FIR luminosity corresponding to the 5σ detection limits of SKA2-MID and SKA1-MID (solid and dashed lines, respectively), as a function of redshift.

various redshifts in Fig. 2, where the galaxy luminosity is indicated by the far-infrared (FIR) luminosity (the total luminosity emitted by dust, which could be compared to the 8–1000 μm luminosity). The FIR–radio correlation in Totani & Takeuchi (2002) is used for the relation between FIR and radio luminosities (see Section 3.4.2 for details).

Although we emphasized high-frequency surveys above, we must mention that tracing both free–free and synchrotron components is the strong point of the wide frequency coverage of SKA. The synchrotron component provides independent information from the free–free component, since it depends on the magnetic field strength in the ISM. Therefore, decomposing those two components serves as a tracer of not only star formation but also amplification of magnetic field.

3 Studies by SKA-Japan Members

We introduce the strong point in the studies of galaxies in Japan. Observationally the rich and deep knowledge and experience of radio astronomy accumulated by Nobeyama Radio Observatory etc. Especially we have a practical advantage to have an access to the ALMA observation time. As being very well-known, ALMA is suitable for observing emissions from dust and various molecules. The combination of such observations and HI data from SKA, we can obtain a global picture of the recycling of the ISM from atomic gas to the SF and metal enrichment via molecular gas. As for the theoretical side, we have a strong point for the simulation of galaxy formation and chemical evolution theory. Thanks to this, as well as theoretical predictions, we can also make a quick comparison when less luminous and/or more distant galaxies are detected by SKA and ALMA.

For the studies of galaxy formation and evolution, we consider three representative redshift ranges. First is the early Universe, in which stars are formed from gas and galaxies grow. namely the nepionic period of galaxies, at $z > 3$. In particular, direct observation of a system with an enormous amount of gas just before the first starburst is crucial to examine the physics of galaxy formation. Second is the epoch in which galaxies establish their global properties through the hierarchical structure formation at $1 < z < 2$. Galaxy morphology emerges in this period. Also the average SFR, fraction of SF activity hidden by dust, and merging rate of dark halos and galaxies peak around this redshift range. Then this is a tumultuous time of galaxy evolution. The last but not least, the important epoch is $z = 0$. Though it looks paradoxical, the *evolution* can be discussed only when the zero-point, the property of nearby galaxies, is well defined. The Local Universe is also important to make a crossover of the ISM physics and extragalactic physics, to construct a large flow of ISM–nearby galaxies–high-z galaxies. We introduce our scientific themes related to these three epochs in the following.

3.1 Nearby Galaxies: Evolution and Characteristics of the ISM and Unified Understanding of Star Formation

Here we describe the science targets that Japan will pursue using SKA in the subject of nearby ($\sim$10 Mpc) galaxy studies. In particular, we focus on (1) the understanding of "dark gas", which is believed to be the dominant component in the transition phase between the atomic and molecular gas, and (2) formation of stars from atomic gas in low metallicity environments. The discussion provided here is naturally linked to the SKA-JP ISM subgroup.

3.1.1 Dark Gas

The 21 cm line has been used as a gas mass tracer under the assumption that the line is optically thin. Contrary to this assumption, Fukui et al. (2015) suggests the presence of optically thick atomic gas in about 50% of the gas traced in 21 cm observations, based on their detailed comparison between the distribution of dust (from Planck) and H I data. They further suggest that this optically thick gas is the component that dominates the density range of 100 - 1000 cm^{-3}, and undetected in CO or 21 cm observations ("dark gas"). The important future direction is to

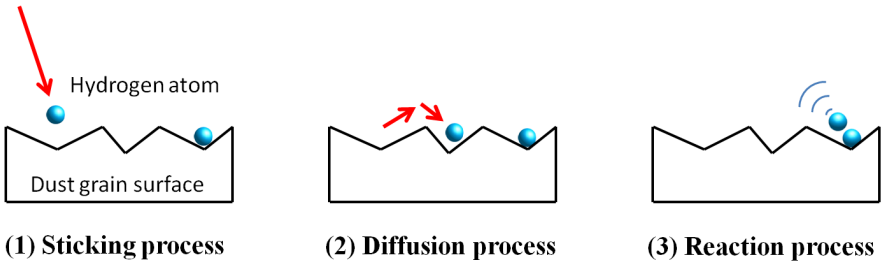


Fig. 3. The four processes for molecular gas formation on dust particles (adopted from Takahashi 2000).

compare the amount/distribution/kinematics of the ionized/atomic/molecular gas (including dark gas) in galactic and extra galactic sources. Pioneering studies have been conducted using the Nobeyama 45m telescope (e.g. Nakanishi et al. 2006; Tosaki et al. 2011; Kaneko et al. 2013), The Milky Way galaxy is the best target for a detailed comparison between the galactic structure and the characteristics of the ISM, but our location in the Galaxy prevents us to conduct such a detailed study. The large scale structure such as spiral arms or bar structure can have a significant effect on the physical condition of the galactic ISM. SKA will allow us to study a typical grand-design spiral galaxy located at 10 Mpc using ~ 0.1 arcsec (5 pc) angular resolution. An important science synergy is to compare the atomic gas distribution obtained with SKA, and the dust distribution obtained with ALMA in nearby spiral galaxies.

The metallicity, which is proportional to the amount of dust, affects the physical condition of the ISM in galaxies, in addition to the kinematical disturbance mentioned above. From recent theoretical studies, it is found that the molecular ISM is not the necessary condition for star formation, but the atomic gas can also lead to star formation in low metallically environments. Therefore, detailed understanding of the atomic gas in the diffuse outskirts of galaxies or dwarf galaxies can be one of the science goals of SKA. We summarize the current understanding of the atomic to molecular transition and the associated star formation, following the review provided by Krumholz (2013), in what follows.

3.1.2 Formation of Stars From Atomic Gas in Low Metallicity Environments

In nearby galaxies, the star formation rate is well correlated with molecular gas, but the correlation with atomic gas is rather poor (Wong & Blitz 2002; Kennicutt et al. 2007; Bigiel et al. 2008; Leroy et al. 2008). The gas depletion time scale $t_{\rm dep}$, which is the ratio between molecular gas mass and star formation rate, is nearly constant in nearby galaxies (~ 2 Gyr; Bigiel et al. (2011)).

The balance between molecular gas formation and dissociation determines the chemical condition of the interstellar hydrogen (Omukai et al. 2012). Molecular gas formation occurs on the surface of dust if the metallically is higher than 1/100,000 of the solar value. The dissociation rate under a typical solar UV radiation is 5×10^{-11} $\rm s^{-1}$ per one hydrogen molecule (Draine & Bertoldi 1996), while the formation rate under a molecular hydrogen column of 100 $\rm cm^{-3}$ is 3×10^{-15} $\rm s^{-1}$ per one hydrogen molecule. Therefore, the predicted molecular hydrogen abundance is only 10^{-4}, if this formation and dissociation balance is maintained. In reality, the Lyman-Werner UV photons are efficiently shielded by the presence of dust, allowing molecular clouds to form. Thus atomic hydrogen dominates the exterior region where the effect of dust attenuation is negligible, while the inner regions are more dominated by the molecular gas due to the abundance of dust (e.g., van Dishoeck & Black 1986; Sternberg 1988; Neufeld & Spaans 1996; Liszt 2002; Glover & Mac Low 2007; Krumholz et al. 2008; Gnedin et al. 2009; McKee & Krumholz 2010; Mac Low & Glover 2012).

The chemical and thermal condition of the interstellar hydrogen gas are both related to the shielding of UV light due to interstellar dust, and this may be the reason for the good correlation between molecular gas and star formation. The chemical condition is determined by the balance between molecular hydrogen formation on dust particles and the photo dissociation due to UV photons. The thermal condition is determined by the balance between the combination of photoelectric heating due to UV photons and the thermal exchange of dust/gas and the cooling due to line emission after collisional excitation. Therefore, the dependence of thermal/chemical process to the volume/column density and the UV radiation field are extremely similar. The cooling rate and the formation rate are both proportional to the density and metallically ($n^2 Z'$), because the cooling due to line emission and the formation of molecular hydrogen are both due to collisions. The UV dissociation and photoelectric heating are both dependent on the UV radiation field and dust attenuation in the same way.

Because of this similarity, the correlation holds well

in a wide range of gas densities, dust attenuation, and metallicity. The transition from atomic to molecular gas occurs at > 100 K to 10 K, and this is determined by the attenuation of dust: the temperature is low in regions where dust attenuation is efficient whereas the temperature is high in regions with little dust attenuation. Therefore, molecular hydrogen and star formation show a good correlation: the transition from atomic to molecular hydrogen is not directly related to the triggering of star formation, but it is rather related to the decrease in gas temperature.

In low metallicity environments, the timescale for the transition from atomic to molecular hydrogen is comparable to the dynamical timescale, but the timescale to reach thermodynamical equilibrium is 1/1000 shorter. The chemical and thermal timescales both depend on the metallicity, and they are longer in low metallicity environments. On the other hand, the timescale for star formation does not depend on metallicity. Therefore there must exist a certain value of metallicity that satisfies a condition in which (thermal timescale) $<$ (dynamical timescale) $<$ (chemical timescale). This suggests that star formation occurs before interstellar hydrogen becomes molecular, if the process that governs star formation is indeed the chemical condition and not the thermal condition. In such a condition, the star formation rate should correlate better with atomic hydrogen rather than atomic hydrogen. This is also suggested in the numerical simulations by Glover & Clark (2012), and further suggested in the analytical model by Krumholz (2012) that this effect is seen in the ISM with metallicities of 1-10% of the solar value.

The SKA-JP galaxy evolution subgroup will collaborate with the ALMA group, and investigate the spatial distribution of the atomic-molecular transition as a function of metallicity and galaxy evolution stage with a future goal to compare the physical processes with the galaxies in the high-z universe.

3.2 Construction and understanding of the extended scaling laws of galaxies connecting gas, dust, and SF

Once the main body of a galaxy has established, a tight relation between some global properties of galaxies emerges. This is referred to as the scaling relation, playing an important role to study the evolution of galaxies. The best-known scaling relation may be the above mentioned TF and BTF relations. There are also many other scaling relations. However, we should note that most of them are heuristic relations without physical explanation. Here we introduce some scaling relations tightly connected to the galaxy evolution, and discuss the way to a synthesis and theoretial reasoning of these relations.

As we mentioned, the SFR is the most interested physical quantity from the point of view of galaxy evolution. In 2015, the relation that gathers researchers' attention is the so-called "the main sequence of SF galaxies" . This is a tight linear sequence of SF galaxies on the (logarithms of) stellar mass M_*–SFR plane. Historically this is an equivalent to the color–magnitude relation, but since it is presented with more physical quantities like M_* and SFR, the scaling relation of SF galaxies appears very prominently (e.g., Schiminovich et al. 2007, among others). It is not surprising that a trivial scaling relation exists since both are global properties of galaxies. What we should pay attention is that the slope of the linear relation is shallower than unity, meaning the more massive a galaxy is, the less efficient the SF activity becomes. This trend is referred to as the downsizing, which was recognized in late 1980's but has not been physically understood until now.

Starburst galaxies like ultraluminous infrared galaxies (ULIRGs) do not locate on the main sequence, but distribute more than an order of magnitude above it (e.g., Buat et al. 2005, 2007). This implies that the main sequence is the relation of quiescently evolving SF galaxies, or the staying time is long in the sequence. Galaxies that already stopped their SF has SFR ~ 0 and do not appear on this plane. Therefore, studies from various point of view are necessary to understand the relation. Genzel et al. (2012) examined the amount of molecular gas in the SF main sequence galaxies. The redshifts of their sample is at $0 < z < 2$, but it is not yet a systematic statistical study. Magnelli et al. (2012) and Magnelli et al. (2014) examined the relation between the temperatures of dust and molecular gas in the main sequence galaxies. However since the observational data of HI is limited to $z < 0.5$ at this moment, it is difficult to discuss its evolutionary aspect. Also in relation between the main sequence and the Kennicutt–Schmidt law discussed in the following, a spatially resolved analysis of galaxies is necessary (e.g., Teruya & Takeuchi 2014). Studies to reveal the mechanism which shapes the main sequence of SF galaxies in terms of the ISM physics will only be possible with ALMA and SKA.

The SF is mainly determined by relatively local conditions of the ISM in galaxies However, it has been well known that the SF and integrated properties of a galaxy are correlated (e.g., Roberts & Haynes 1994; Kennicutt & Evans 2012). The existence of a correlation between local properties, like the spiral arms, molecular clouds, HII

regions, etc., and global properties like the morphology, total mass, etc., is not a trivial phenomenon at all but an important problem to be solved by the astrophysics. A relation between the (surface) densities of gas and SFR, which appears in various spatial scales, is the Kennicutt–Schmidt (KS) law (see e.g., Kennicutt & Evans 2012, as a review). The KS law is expressed as follows:

$$\Sigma_{\rm SFR} \propto \Sigma_{\rm gas}^{n} \, . \tag{2}$$

This relation is a single power law for more than six orders of magnitude. The index n is observationally in a range of $1 < n < 2$. Whether n is closer to 1 or 2 determines the plausible scenario of the physical process in a molecular gas to form stars (e.g., Momose et al. 2013). The KS law is an important ingredient in the theory of chemical evolution in galaxies, and gives a great impact if it will be physically understood. Thus, the KS law is of great interests from ISM to the extragalactic physics.

However, we should point out that still the KS law is a purely empirical relation. Further, the debate on the index n is not yet converged. In order to derive the KS law from physical processes like the gravitational collapse and/or collision of molecular clouds, a large galaxy sample with neutral and molecular gas information selected by a homogeneous criterion is necessary to present the relation with errors as small as possible. SKA will play a unique role utterly impossible with other instruments. With the sample obtained by SKA, we can explore the spatially resolved KS law up to $z \sim 1$ and clarify the governing physical processes. By synthesizing the all scaling laws, we will find a unified scaling law of galaxies. We try to derive this unified relation from a first principle. Studies on galaxy evolution will be mature by such an approach.

3.3 Exploration of galaxy evolution through H I 21-cm absorption lines

As discussed in Section 2.6, gas absorption in the lines of sight of bright continuum sources such as QSOs will enable us to trace the ISM and IGM at various redshifts. In particular, Lyα absorption line systems are often used for such studies. There have been some attempts of detecting 21 cm absorption in DLAs (Lyα absorption systems with $N_{\rm HI} > 2 \times 10^{20}$ cm^{-2}), but most of the DLAs are not detected, indicating small $\tau_{21\,\rm cm}$. This suggests that a large fraction of the area of the ISM in the intervening systems is covered by the warm ISM, whose typical temperature is higher than 1,000 K (equation 1).

A high covering fraction of the warm ISM in DLA hosts is also suggested by Hirashita et al. (2003, hereafter H03), who interpreted the small fraction of H_2 (Lyman-Werner band absorption) detection for DLAs as due to the predominant warm medium in which the equilibrium H_2 fraction ($f_{\rm H_2}$: the fraction of hydrogen nuclei in the form of H_2) is as low as $\lesssim 10^{-6}$. Indeed, from some observations, although the H_2 fraction is largely enhanced for some DLAs, stringent upper limits ($f_{\rm H_2} \lesssim 10^{-7}$–$10^{-5}$) are laid on a significant fraction of DLAs (Black, Chaffee, & Foltz 1987; Petitjean, Srianand, & Ledoux 2000). This can also be interpreted as due to a low formation rate of H_2 in dust-poor environments relative to the Milky Way (Levshakov et al. 2000; Ledoux, Petitjean, & Srianand 2003; Petitjean et al. 2006) or a high H_2 dissociation rate by strong UV radiation (Petitjean et al. 2000). However, we should keep in mind that such upper limits do not exclude the existence of molecule-rich clouds in these systems, because such clouds may have a very low volume filling factor and may be rarely located in the line of sight as shown by our study above (H03). Therefore, it appears that the ISM structures, in which dense regions are localized while most of the volume is occupied by the warm diffuse medium, provide a common interpretation for the lack of detections in both H I 21 cm absorption and H_2 in DLAs.

One of the possible contributions from the SKA-Japan community is to provide a numerical simulation scheme which can predict the statistics of 21 cm line optical depth based on high-resolution density and temperature structures and chemical reactions (especially H_2 formation on dust). High-resolution simulations of the ISM in the cosmological structure formation scenario have been performed by e.g., Saitoh et al. (2009), Okamoto (2013), and Yajima et al. (2015). These simulations will enables us to obtain a tool for interpreting the statistics of $\tau_{21\,\rm cm}$ through its dependence on $N_{\rm HI}$ and $T_{\rm s}$ (equation 1). We could also implement chemical reactions of other species such as CO based on the formulation by Inoue et al. (2007), who considered gamma-ray bursts instead of QSOs for background sources. Moreover, the treatment of H_2 formation on dust could be refined based on recent efforts on implementing dust enrichment and H_2 formation in galaxy evolution simulations (Bekki 2015). Detailed modeling of dust enrichment by Asano et al. (2013) could be implemented in the simulations. These lines of modeling will enable us to make a unique contribution to H I absorption studies by SKA.

In the following, we demonstrate that modeling of the ISM based on a high-resolution simulation is useful to interpret the 21 cm absorption statistics. We use our previous 2-dimensional model in H03 for a first step, since it was used in our previous studies to interpret the paucity of H_2 detection in DLAs. The results will be used as a

basis for a future development using the state-of-the-art simulations mentioned above. Braun (2012) adopted the observational H I maps of nearby galaxies with a typical spatial resolution of 15–100 pc and predicted the statistics of $\tau_{21\ \mathrm{cm}}$ for DLAs. However, we are also interested in the H_2 abundance, and it is difficult to get observational H_2 map down to the level of $f_{H_2} \sim 10^{-6}$ (typical detection limit for DLAs) even for nearby galaxies. The theoretically made H_2 map by H03 can serve to overcome this difficulty. Since H_2 formation is related to the dust abundance (see e.g. Fynbo et al. 2011), we can also include the bias in the optical selection of QSOs caused by dust extinction in a self-consistent way. We use the same values as in H03 for the cosmological parameters: $(h, \Omega_\mathrm{m}, \Omega_\Lambda, \Omega_\mathrm{b}) = (0.7, 0.3, 0.7, 0.02h^{-2})$.

3.3.1 Simulation of the ISM structures in a DLA host galaxy

We briefly review the hydrodynamical simulation in H03. It is a 2-dimensional hydrodynamical simulation of a galactic disc based on Wada & Norman (2001). We chose the parameter values appropriate for formation redshift $z_\mathrm{vir} = 3$ and virial mass $M_\mathrm{vir} = 8.0 \times 10^{10}\ \mathrm{M}_\odot$. A 1 kpc × 1 kpc area is simulated with 2048 × 2048 grids. We refer the interested reader to H03 for the simulated hydrogen column density (N_H) and gas temperature (T_gas) maps. Although they concentrate on H_2 fraction in DLAs, the same framework is applicable for 21 cm optical depth. To avoid the effect of the boundary conditions we only use the central 450 pc radius. Although the host galaxies of DLAs are not necessarily large disk galaxies, we only use the simulation to model the structures of the ISM created by hydrodynamical evolution. We assume that such hydrodynamical structures are common for possible DLA hosts.

To choose the possible lines of sight for DLAs, we only adopt the grids where $N_\mathrm{H} \geq 2 \times 10^{20} \mathrm{cm}^{-2}$. We also introduce the dust extinction effect, since if the extinction is so large that the background QSO is obscured, such a line of sight cannot sample DLAs. Vladilo & Péroux (2005) showed strong lack of DLAs with zinc column density $N_\mathrm{Zn} > 10^{13.2} \mathrm{cm}^{-2}$, which they explained with the effect of extinction in metal-rich environments. For each of the grids in our simulated galaxy, we calculate N_Zn as $N_\mathrm{Zn} = 10^{-7.35}(Z/\mathrm{Z}_\odot)N_\mathrm{H}$, where the factor $10^{-7.35}$ is the number ratio of Zn to H in the solar composition (Anders & Grevesse 1989) and $Z/\mathrm{Z}_\odot$ is the metallicity normalized to the solar metallicity. We treat the metallicity as a free parameter. We exclude those grids where $N_\mathrm{Zn} > 10^{13.2}\ \mathrm{cm}^{-2}$, consistent with the observed extinction bias mentioned above.

We calculate the optical depth of 21 cm absorption $\tau_{21\ \mathrm{cm}}$ on each grid using equation (1). We assume that $T_\mathrm{s} = T_\mathrm{gas}$, since the density is high enough for the spin temperature to approach the kinetic temperature (Field 1958). We also assume that all hydrogen is in atomic form; i.e. $N_\mathrm{HI} = N_\mathrm{H}$. We adopt $\Delta v = 10\ \mathrm{km\ s}^{-1}$ based on the typical nonthermal velocity dispersions observed in galaxies (Braun et al. 2009). We also calculate a quantity free from the assumptions on Δv by integrating $\tau_{21\ \mathrm{cm}}$ over the entire line profile:

$$\int \tau_{21\,\mathrm{cm}}\,\mathrm{d}v = 0.54 \left(\frac{T_\mathrm{s}}{10^3\,\mathrm{K}}\right)^{-1} \left(\frac{N_\mathrm{H}}{10^{21}\,\mathrm{cm}^{-2}}\right) \mathrm{km\,s}^{-1}. \quad (3)$$

Under a given N_H and T_gas at each grid, we evaluate $f_{H_2} = 2n_{H_2}/n_\mathrm{H}$, where n_H and n_{H_2} are the number densities of hydrogen nuclei and H_2, respectively. The formulae are summarized in section 2.1 of Hirashita & Ferrara (2005). We assume the following equilibrium condition: $R_\mathrm{dust} = R_\mathrm{diss}$, where R_dust and R_diss are the rates of H_2 formation on dust grains and H_2 dissociation by UV radiation per unit volume, respectively. We adopt a dust grain radius of 0.1 μm, a dust material density of 3 g cm^{-3}, and the typical UV radiation field in the solar neighbourhood. The local hydrogen number density is related to the column density as $n_\mathrm{H} = N_\mathrm{H}/H$ (the thickness of disk is assumed to be $H = 100$ pc). Since the dependence of R_dust on the dust temperature (T_d) is weak, we simply adopt $T_\mathrm{d} = 20$ K. For the dust-to-gas ratio, we adopt a scaling relation with the metallicity as $\mathcal{D} = 0.01(Z/\mathrm{Z}_\odot)$.

3.3.2 Results and Comparison with Observations

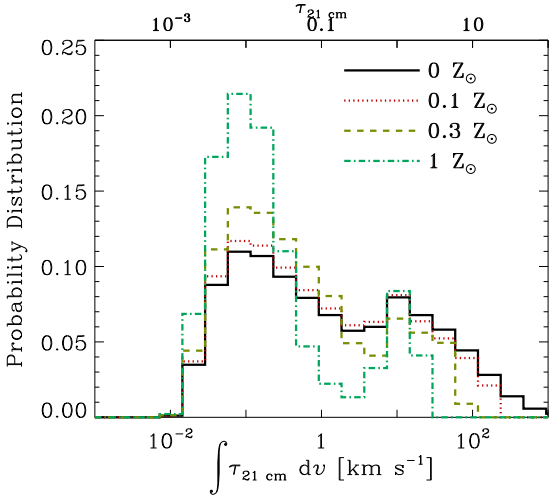


Fig. 4. Probability distribution function of $\int \tau_{21\ \mathrm{cm}}\,\mathrm{d}v$ with various extinctions scaled with the metallicity. The solid, dotted, dashed, and dot-dashed lines show the results for $Z = 0$, 0.1, 0.3, and 1 $\mathrm{Z}_\odot$, respectively. The upper horizontal axis shows $\tau_{21\ \mathrm{cm}}$ with $\Delta v = 10\ \mathrm{km\ s}^{-1}$.

We show the probability distribution function of $\tau_{21\ \mathrm{cm}}$ in Fig. 4. The probability distribution is calculated by counting the number of grids in each logarithmic bin of $\tau_{21\ \mathrm{cm}}$ and normalizing the total probability to unity. For the case without extinction, we clearly find two peaks around $\int \tau_{21\ \mathrm{cm}}\,dv \sim 0.1$ and 10. The higher peak around $\tau_{21\ \mathrm{cm}} \sim 0.01$ is originating from the warm diffuse medium where column density is relatively small (but larger than $2\times10^{20}\mathrm{cm}^{-2}$; Section 3.3.1) with high temperature ($T_{\mathrm{gas}} \gtrsim 10^3$ K), while the lower peak around $\tau_{21\ \mathrm{cm}} \sim 1$ is due to cool and dense regions. We emphasize that the dominant contribution of the warm diffuse component is due to the natural consequence of the compressible hydrodynamical evolution (see also Wada & Norman 2001), not due to the stellar feedback, which we neglected. In other words, the dominant warm diffuse ISM is a natural consequences of the compressible hydrodynamical evolution of the ISM.

We also show the distribution of $\tau_{21\mathrm{cm}}$ with the dust extinction effect for $Z = 0.1$, 0.3, and 1 $\mathrm{Z}_\odot$ in Fig. 4. It is obvious that the abundance dramatically decreases at large $\tau_{21\mathrm{cm}}$ originating from high column density regions where the extinction is large. The peak at $\tau_{21\mathrm{cm}} \sim 0.01$ is relatively enhanced as the extinction bias becomes stronger.

Some features in Fig. 4 match the observational properties of 21 cm absorption in DLAs. A large fraction of DLAs are not detected in 21 cm absorption and typical upper limits of $\tau_{21\ \mathrm{cm}}$ is roughly ~ 0.02 (or $\int \tau_{21\ \mathrm{cm}}\,dv \sim 0.2$ km s^{-1}) (Srianand et al. 2012; Kanekar et al. 2014). The peak of the distribution is at $\tau_{21\mathrm{cm}} \sim 0.01$, explaining well the non-detection. Therefore we conclude that the lack of 21 cm absorption detection for DLAs is due to the combination of two effects: a large covering fraction of the warm diffuse medium and an extinction bias against large $\tau_{21\ \mathrm{cm}} (\gtrsim 1)$. The possible overestimate of the area of dense regions (Section 3.3.1) strengthens our conclusion of the significance of the lines of sight with small $\tau_{21\ \mathrm{cm}}$.

In Fig. 5, we show the cumulative distribution of $\int \tau_{21\ \mathrm{cm}}\,dv$. The cumulative distribution $P(<\int \tau_{21\ \mathrm{cm}}\,dv)$ is defined as the probability of having the integrated $\tau_{21\ \mathrm{cm}}$ smaller than a given value. For the observational data, we refer to Srianand et al. (2012) and Kanekar et al. (2014) with total 48 available DLAs. Since a large fraction of them only have upper limits of $\tau_{21\ \mathrm{cm}}$, we use the upper limits for the observed value (solid line in Fig. 5). Thus, the real distribution should be on the left side of the solid line. Note that these data are not aimed at complete sampling so that our attempt of comparison here provides only a first step for quantitative test.

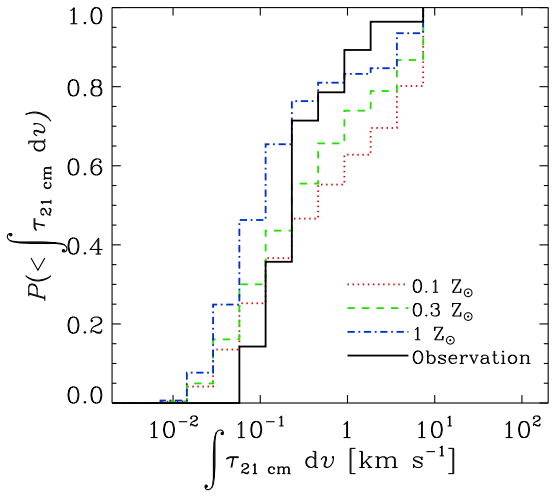


Fig. 5. Cumulative distribution of $\int \tau_{21\mathrm{cm}}\,dv$. The solid line shows the observational distribution constructed by the samples in Srianand et al. (2012) and Kanekar et al. (2014). Note that most of the observational data are upper limits, which are plotted as detected; thus, the real observational distribution should be on the left side of the solid line. The dotted, dashed, and dot-dashed lines show our theoretical results with $Z = 0.1$, 0.3, and 1 $\mathrm{Z}_\odot$, respectively. The result for $Z = 0$ is almost identical with that for $Z = 0.1$ $\mathrm{Z}_\odot$.

From the figure, we conclude that at low $\int \tau_{21\mathrm{cm}}\,dv$, the theoretical predictions are consistent with the observation, since they lie on the left side of the solid line. This again confirms that the lack of detection of 21 cm absorption for DLAs is due to the large area covered by small $\tau_{21\ \mathrm{cm}}$. However, the theoretical prediction overproduces the probability distribution at large $\int \tau_{21\mathrm{cm}}\,dv$. The case with the highest metallicity is the most consistent with the data, since the extinction bias enhances the abundance of DLAs with small $\tau_{21\ \mathrm{cm}}$. The discrepancy may be due to the possible overestimate of the covering fraction of dense regions as mentioned in Section 3.3.1.

3.3.3 Relation between f_{H_2} and $\tau_{21\ \mathrm{cm}}$

Figure 6a shows the probability distribution function of f_{H_2} for various ranges of $\tau_{21\ \mathrm{cm}}$. We simply adopt $Z = 0.1$ $\mathrm{Z}_\odot$, but the metallicity does not change the trend between $\tau_{21\ \mathrm{cm}}$ and f_{H_2}. As expected, there is a trend that large f_{H_2} appears as $\tau_{21\ \mathrm{cm}}$ becomes larger.

At $\tau_{21\ \mathrm{cm}} > 0.02$ for which the current typical sensitivity could detect 21 cm absorption, the scatter of f_{H_2} is large as shown in Fig. 6a. Moreover, the peak still lies at $f_{\mathrm{H}_2} < 10^{-6}$ even for $\tau_{21\ \mathrm{cm}} > 0.02$. On the other hand, a small $\tau_{21\ \mathrm{cm}}$ implies a low f_{H_2} ($\lesssim 10^{-6}$). Fig. 6b shows the probability distribution function of $\tau_{21\ \mathrm{cm}}$ for various ranges of f_{H_2}. We observe that the distribution shifts to-

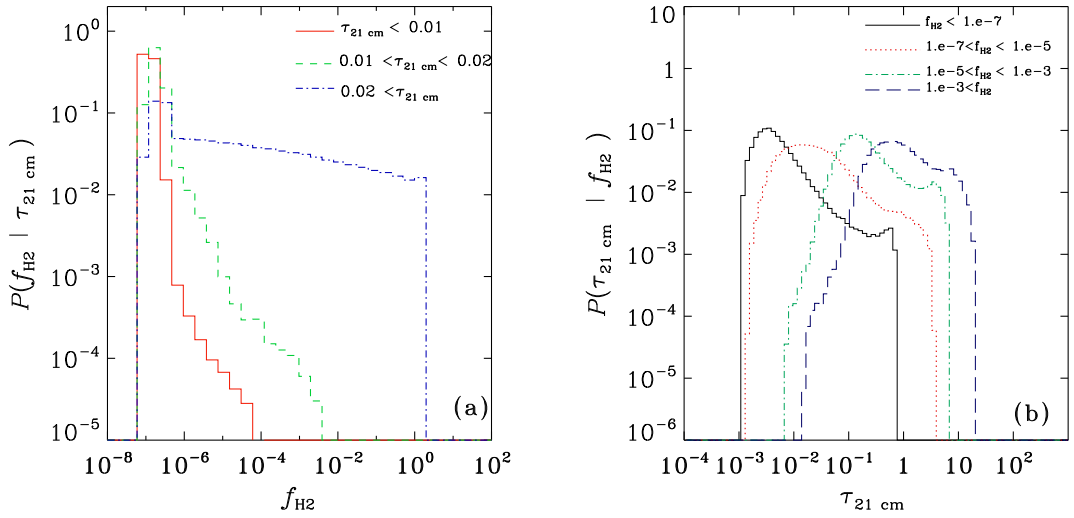


Fig. 6. (a) Distribution function of $f_{\mathrm{H_2}}$ for $\tau_{21\ \mathrm{cm}} < 0.01$ (solid line), $0.01 < \tau_{21\ \mathrm{cm}} < 0.02$ (dashed line), and $\tau_{21\ \mathrm{cm}} > 0.02$ (dot-dashed line). (b) Distribution function of $\tau_{21\ \mathrm{cm}}$ for $f_{\mathrm{H_2}} < 10^{-7}$ (solid line), $10^{-7} < f_{\mathrm{H_2}} < 10^{-5}$ (dotted line), $10^{-5} < f_{\mathrm{H_2}} < 10^{-3}$ (dot-dashed line), and $f_{\mathrm{H_2}} > 10^{-3}$.

ward larger $\tau_{21\ \mathrm{cm}}$ as $f_{\mathrm{H_2}}$ becomes larger. This indicates that, if we choose DLAs with $f_{\mathrm{H_2}} \gtrsim 10^{-3}$, there is a large probability of detecting 21 cm absorption. On the other hand, small $f_{\mathrm{H_2}} < 10^{-5}$ does not necessarily mean that detection of 21 cm absorption is hard, since there is a significant tail toward $\tau_{21\ \mathrm{cm}} > 0.02$ even for $f_{\mathrm{H_2}} < 10^{-5}$.

Our theoretical predictions are summarized as follows: (i) non-detection of 21 cm absorption ($\tau_{21\ \mathrm{cm}} \lesssim 0.02$) indicates a small $\mathrm{H_2}$ fraction ($f_{\mathrm{H_2}} \lesssim 10^{-6}$). As a corollary of this, a large $\mathrm{H_2}$ fraction (especially $f_{\mathrm{H_2}} \gtrsim 10^{-3}$) favours a detectable 21 cm absorption. (ii) Detection of 21 cm ($\tau_{21\ \mathrm{cm}} \gtrsim 0.02$) does not necessarily mean a large $\mathrm{H_2}$ fraction. As a corollary of this, a small $\mathrm{H_2}$ fraction ($f_{\mathrm{H_2}} \lesssim 10^{-5}$) does not necessarily lead to a non-detection of 21 cm absorption. These two predictions are broadly supported by the existing sample in Srianand et al. (2012) and Kanekar et al. (2014), although the number of sample (~ 10) is small. The exception for (i) is the DLAs associated with J040718.0−441013 ($z_{\mathrm{abs}} = 2.59475$; $\int \tau_{21\ \mathrm{cm}} \mathrm{d}v < 1.61$ km s^{-1} and $\log f_{\mathrm{H_2}} = -2.61$) and with J053007.9−250330 ($z_{\mathrm{abs}} = 2.81115$; $\int \tau_{21\ \mathrm{cm}} \mathrm{d}v < 0.58$ km s^{-1} and $\log f_{\mathrm{H_2}} = -2.83$). However, the upper limits for $\tau_{21\ \mathrm{cm}}$ is still large (0.16 and 0.058, respectively, if we assume $\Delta v = 10$ km s^{-1}). The prediction (ii) is supported by the current sample. We need to test these predictions by a larger sample, which would be a critical test for our theory.

3.3.4 Requirement for future 21-cm absorption observations of DLAs

As shown above, a large part of DLAs are predicted to have $\tau_{21\ \mathrm{cm}} \lesssim 0.01$ down to 10^{-3}. Therefore, in order to detect 21 cm absorption of a major part of DLAs with 3 σ, we need to achieve a signal-to-noise ratio of 3000 (i.e., a spectral dynamic range of 35 dB). Assuming a typical flux of 100 mJy for background QSOs (Srianand et al. 2012), a root-mean-square (rms) noise level of 33 nJy is required. The current rms achieved by GBT and GMRT is typically a few mJy for an integration time of ~ 10 h (e.g., Srianand et al. 2012). A 100 times larger collecting area compared with the currently available large radio telescopes, the same integration time would achieve an rms of a few $\times 10$ nJy. SKA would have this kind of large collecting area.

3.4 Tracing the star formation activities with radio continuum

We have been contributing to the studies of galaxy evolution in the radio through modeling of galaxy number count (Takeuchi et al. 2001) and of spectral energy distribution (SED) (Totani & Takeuchi 2002; Hirashita & Hunt 2006). We also plan a survey observation based on our submillimetre galaxy survey being or to be planned.

3.4.1 SED models of young starbursts

As mentioned in Section 2.7, SKA is sensitive enough to conduct wide-area surveys at $\gtrsim 10$ GHz, a relatively high frequency unexplored for wide-area deep surveys. At

such a high frequency, the relative contribution of free–free emission to synchrotron emission is larger than at lower frequencies. In particular, the importance of tracing free–free emission is pronounced if we target young starbursts. Indeed, some authors have shown that the radio SEDs of nearby young starbursts have flat slopes, which can be interpreted as being dominated by free–free emission (Deeg et al. 1993; Roussel et al. 2003; Hunt et al. 2005). However, the dependence of radio spectral index on age has not been clarified yet, especially for high-redshift galaxies. The wide-band coverage of SKA is suitable to systematically survey the evolution of radio spectral index as a function of redshift.

One of the ongoing activities of SKA-Japan is to model the radio SED based on an empirical approach using the radio–FIR relation (Takeuchi et al. 2001) or based on a theoretical approach treating the evolution of H II regions and supernova remnants in a consistent manner with the star formation history (Hirashita & Hunt 2006; Hirashita 2011). One of the results applied to the central starburst in a nearby blue compact dwarf galaxy, II Zw 40, is shown in Figure 7. We give the total gas mass M_0 and initial hydrogen number density $n_{\rm H0}$, and evaluate the star formation rate as a function of time as $\psi(t) = (\epsilon_{\rm SF} M_0/t_{\rm ff}) {\rm e}^{-\epsilon_{\rm SF} t/t_{\rm ff}}$, where we adopt the star foramtion efficiency $\epsilon_{\rm SF} = 0.1$ and the free-fall time $t_{\rm ff}$ estimated by $n_{\rm H,0}$. The emission measure of the ionized region, which is necessary to calculate the free–free component, is estimated consistently with the total number of ionizing photons produced by massive stars and the change of hydrogen number density $n_{\rm H}$ by the pressure-driven expansion. The synchrotron component is also included based on the calculated number of supernova remnants. Free–free absorption, which is important at low frequencies, is also considered.

In Figure 7a, we show the radio SEDs at $t = 1$, 3, and 5 Myr with $n_{\rm H0} = 10^5$ cm^{-3} and $M_0 = 3 \times 10^6$ M$_\odot$. As the age becomes older, the peak shifts to lower frequencies, because the free-free optical depth becomes smaller as the H II region expands (the decline of the flux at low frequencies is due to free–free absorption). At $t = 1$ and 3 Myr, the emission is completely dominated by free–free emission, and at $t = 5$ Myr, the synchrotron component begins to contribute to the emission and the spectrum slope changes. For comparison, the VLA 'matched' data whose (u, v) coverage is restricted to baselines greater than 20kλ (i.e., sensitive to structures smaller than $4''$) are adopted (three triangles in Fig. 7) as representative fluxes from the central star-forming region.

The density strongly affects the frequency at which the flux peaks because free–free absorption is sensitive

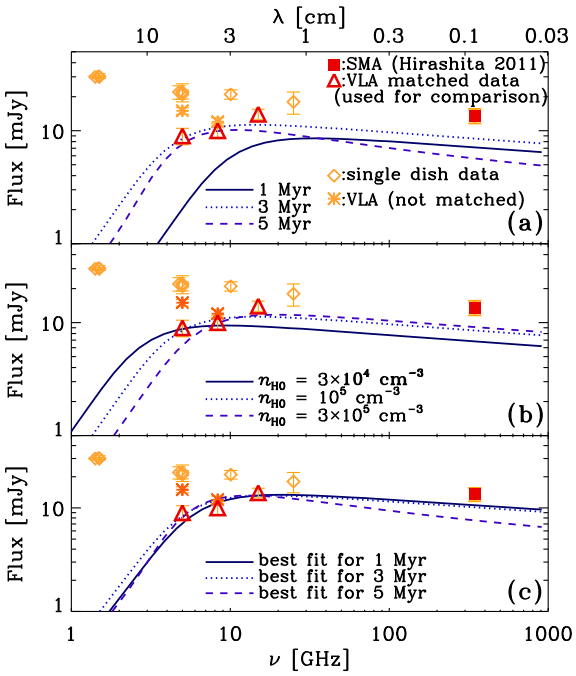


Fig. 7. Radio SEDs for the central ($4''$) starburst in II Zw 40 (Hirashita 2011). (a) Solid, dotted, and dashed lines show the SEDs calculated by the theoretical model for ages 1, 3, and 5 Myr, respectively. The initial hydrogen number density and the total mass converted into stars are fixed with $n_{\rm H0} = 10^5$ cm^{-3} and $M_0 = 3 \times 10^6$ M$_\odot$, respectively. The filled square represents our Submillimeter Array (SMA) measurement at 880 μm for the central star-forming region (Hirashita 2011). Diamonds show single-dish measurements by Jaffe et al. (1978), Klein et al. (1984), and Klein et al. (1991), while asterisks at 6 and 3.6 cm are the VLA fluxes synthesized by all the (u, v) data, which are sensitive to structures up to 10 arcsec and 7 arcsec, respectively (Beck et al. 2002): these data are also senstive to emissions more extended than the central star-forming region. The triangles at 6, 3.6, and 2 cm are the matched VLA fluxes obtained by restricting (u, v) data to baselines greater than 20kλ (i.e., sensitive to the structures smaller than $4''$) (Beck et al. 2002). We compare the models with these data (triangles). (b) Same as Panel (a) but for the SEDs at 3 Myr with various initial densities. Solid, dotted, and dashed lines are for $n_{\rm H0} = 3 \times 10^4$, 10^5, and 3×10^5 cm^{-3}, respectively ($n_{\rm H} = 1.8 \times 10^3$, 3.2×10^3, and 5.4×10^3 cm^{-3} at 3 Myr, respectively; since we consider the expansion of H II region, the density becomes lower than the initial value). (c) Same as Panel (a) but for the best-fit model parameters $(M_0\,[{\rm M}_\odot], n_{\rm H0}\,[{\rm cm}^{-3}]) = (1.1 \times 10^7, 2.2 \times 10^4)$, $(3.5 \times 10^6, 1.2 \times 10^5)$, and $(4.1 \times 10^6, 1.2 \times 10^5)$ at three given ages, 1, 3, and 5 Myr, for the solid, sotted, and dashed lines, respectively. The fitting is applied for the three triangles (the matched VLA fluxes).

to the density. In Fig. 7b, we show the SEDs at $t = 3$ Myr for various initial densities ($n_{\rm H0}$) with $M_0 = 3 \times 10^6$ $M_\odot$. We observe that the peak position of the SED is indeed sensitive to the density. The rising spectrum of the matched data (triangles) is consistent with free–free absorption.

It is possible to search for the best-fit values of M_0 and $n_{\rm H0}$ for each age. The matched VLA data are adopted (three triangles in Fig. 7) for the χ^2 fitting, since our models are applicable to the central star-forming region. The best-fit solutions are shown in Fig. 7c. As seen in Fig. 7c, the spectral slope at $\nu \gtrsim 15$ GHz at $t = 5$ Myr is different from that at $t \leq 3$ Myr because of the contribution from the synchrotron component.

If the age is about 3 Myr as suggested from the optical and near-infrared observations (Vanzi et al. 2008), 75 per cent of the 880 μm flux obtained in the SMA observation (Hirashita 2011), which is sensitive to the central starburst, is explained by free–free emission according to the best-fit SED at 3 Myr (the flux at 880 μm is 10.2 mJy in the model, while the observed flux is 13.6 mJy). The difference ($\simeq 3.4$ mJy) is likely to be due to the dust and/or diffuse (i.e., not associated with the compact H II region) free–free emission.

The above example indicates that, if we focus on the young starburst, the radio emission can be dominated by free–free emission. At the same time, if the starburst is occuring in a dense and compact region, which is likely because of the short free–fall time-scale, emission at $\lesssim 10$ GHz could be significantly affected by free–free absorption. Therefore, if we would like to trace a young starburst, it would be desirable to target frequencies > 10 GHz.

3.4.2 Radio survey and combination with submm data

Utilizing the galaxy survey data already taken by ALMA could make a strong scientific case, especially because Japan has access to ALMA. Submm surveys, which will be conducted by ALMA, are always affected by some bias caused by dust temperature, as shown below. In contrast, radio surveys at frequencies that SKA can access have an advantage of avoiding a bias caused by dust temperature, if we assume that the radio–FIR relation always holds. (In fact, we should keep in mind that there are other complications at radio wavelengths such as the variation of spectral slope, or the relative ratio between free–free and synchrotron emissions.)

Before considering an SKA survey, we investigate what kind of preparatory survey can be performed by ALMA. We focus on 350 GHz ($\lambda = 850$ μm) for the target frequency, but using a wavelength around 1 mm does not change the conclusions below. A shorter wavelength has much lower efficiency because of a smaller field of view (FoV) and less chance of suitable atmospheric conditions. The largest disadvantage of ALMA is a narrow FoV ~ 0.047 arcmin^2 at 350 GHz (assuming a primary beam of 12-m dish), which makes the survey efficiency extremely low. On the contrary, SKA has a wide FoV. SKA-MID has a FoV ~ 37 arcmin^2 (assuming a primary beam of 15-m dish). Therefore, ALMA needs 790 pointings to cover a FoV of SKA.

Now let us assume that an on-source observational time is 1,000 hr for both SKA and ALMA. Such a long observational time may be appropriate for future legacy observations of both telescopes. Then, we can spend 1.3 hours per field by ALMA. Using the ALMA sensitivity calculator[3], root mean squeare $\sigma \simeq 16$ μJy is achieved with 60 antennas at 350 GHz. Therefore, we adopt 80 μJy (5σ) for the detection limit. On the other hand, we adopt a 5σ detection limit of 0.2 μJy at 10 GHz for SKA1-MID and 0.02 μJy at 10 GHz for SKA2-MID (e.g., Murphy et al. 2015), for an integration time of 1,000 hr. The detection limit flux of SKA1-MID is 10 times larger.

To clarify the population expected to be detected at the ALMA survey described above, we show the relation between the dust temperature, $T_{\rm d}$, and the total IR luminoisity (total luminosity emitted by dust, which could be compared to the 8–1000 μm luminosity), $L_{\rm FIR}$, in Figure 8, adopting the 5σ detection limit, 80 μJy, at 350 GHz. We adopt the FIR–radio SED model by Totani & Takeuchi (2002), who give the SED under given $T_{\rm d}$ and $L_{\rm FIR}$. They also empirically included radio emission by assuming the observed radio–FIR correlation in nearby galaxies.[4] In Figure 8 (upper panel), we plot the minimum $L_{\rm FIR}$ detected for an object with a dust temperature $T_{\rm d}$; that is, objects with the FIR luminosity larger than the minimum (or the right side of the curve) can be detected. From Figure 8, we observe that the ALMA 350 GHz survey does not have strong redshift dependence for the dust temperatures usually observed (> 20 K), which is due to the so-called negative K-correction, and that the sample is strongly biased against high $T_{\rm d}$. This kind of bias was already pointed out by Chapman et al. (2005). On the other hand, SKA2-MID 10 GHz detection limit does not depend on dust temperature, and is only deter-

[3] https://almascience.eso.org/proposing/sensitivity-calculator

[4] If we simply use the radio–FIR relation to estimate the radio luminosity from the total FIR luminosity, the radio flux should not depend on the dust temperature. However, Totani & Takeuchi (2002)'s model, which we adopt, has a weak dependence of dust temperature through their equation 11. To avoid this dependence we always adopt a fixed value for $T_{\rm dust} = 30$ K in calculating the 10 GHz flux.

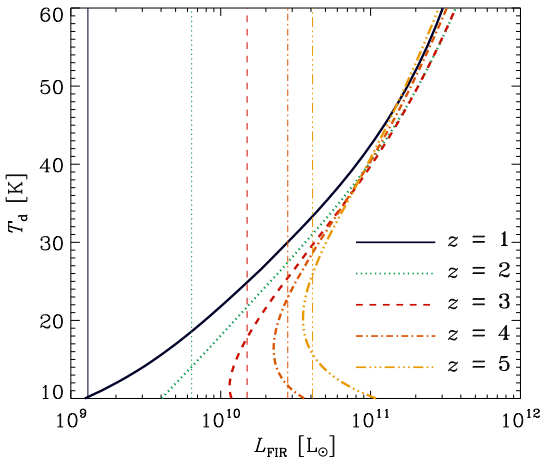


Fig. 8. Dust temperature (T_d) vs. total FIR luminosity (L_{FIR}) corresponding to the detection limits for ALMA (350 GHz) and SKA2-MID (10 GHz) under the condition that a FoV of SKA2-MID (30 arcmin^2) is surveyed in an on-source integration time of 1,000 hr. The solid, dotted, dashed, dot-dashed, triple-dot-dashed lines present the 5σ detection limits galaxies at $z = 1$, 2, 3, 4, and 5, respectively. Objects whose total FIR luminosity is larger than (i.e., on the right side of) each line are detected. The thick curves are for ALMA and the thin vertical lines are for SKA2-MID. The detection limit for SKA1-MID can be easily estimated by shifting each line for SKA2-MID by 10 times towards larger L_{FIR}.

mined by FIR luminosity in our model.

In Figure 8, we observe that SKA2-MID has a similar sensitivity to ALMA in terms of L_{FIR} at $z \gtrsim 3$ if we assume a normal dust temperature (20–40 K). Therefore, the combination of these two surveys are suitable to investigate the evolution of radio–FIR survey at $z \gtrsim 3$. At the same time, SKA2-MID is also capable of studying a population of low-L_{FIR} ($L_{FIR} \lesssim 10^{11}$ $L_\odot$) galaxies with high dust temperature $T_{dust} \gtrsim 30$ K, which are missed by ALMA surveys. SKA1-MID, which has a ten times worse sensitivity than SKA2-MID, is suitable to study galaxies at $z \lesssim 2$ detected by ALMA surveys.

4 Summary

Galaxies have been formed from a homogeneous neutral gas in the early Universe, and evolved with forming stars from the gas in them. Then the key factor of the galaxy formation and evolution is the transition from atomic to molecular hydrogen. This transition is also strongly coupled with chemical evolution, because dust grains play a critical role in molecular formation. Therefore, a comprehensive understanding of neutral–molecular gas transition, star formation and chemical enrichment is necessary to clarify the galaxy formation and evolution.

The SKA-Japan galaxy evolution subSWG is working on the following topics among vast variety of interesting unsolved problems in this field. At $z \sim 0$, we try to construct a unified picture of atomic and molecular hydrogen through nearby galaxies in terms of metallicity and other various ISM properties. In previous studies, the knowledge from the ISM physics was not efficiently used in extragalactic stuies, mainly because of the limitation of the angular resolution in radio observations today. The ultimately high high angular resolution of SKA at cm wavelengths will bring us the unprecedented information of the physical state of the ISM in galaxies. By SKA, we will be able to push forward the H I–H_2 transition toward significantly high-z and discuss its evolution.

Up to intermediate redshifts $z \sim 1$, we explore scaling relations including gas and star formation properties, like the main sequence and the Kennicutt–Schmidt law of star forming galaxies. To connect the global studies with spatially-resolved investigations, such relations will be plausibly a viable way. Especially in relation to the H I–H_2 topic, the Kennicutt–Schmidt law provides a unique opportunity, since this relation holds both for resolved (local) and global galaxy properties. If we can trace the evolution (or constancy) of these scaling relations, we can constrain the star formation scenarios in galaxy evolution. It is particularly important since it is the way how to connect the ISM physics and extragalactic physics and organize them on the common basis. Only SKA can achieve such observations.

At high redshift, it would be very difficult to detect the H I emission of galaxies, even with SKA2. Instead, the absorption lines of HI 21-cm line will be a very promising observable to explore the properties of gas in galaxies. We are interested in the physical processes going on during the galaxy formation. One of the ideal proves for this is a high column density system like DLAs. Though DLAs are alreacy extensively studied in the field of galaxy formation and cosmology, one possible bias was pointed out. If a DLA contains even a tiny amount of dust, it would bias the detection probability of background quasars. This plausible bias can be compensated by selecting radio-loud quasars and explore the 21-cm absorption line system. Since the cross section of such system is small, we can examine their physical properties even if the column density is extremely high.

Apart from H I, we have yet another great probe for the star formation history in the whole range of the cosmic time. The radio continuum at $\nu \gtrsim 10$ GHz consists of thermal free-free and synchrotron emission. Both of these radiation processes are related to the star formation activity in galaxies, and work as a good tracer of the SFR. Since the feasibility of the radio continuum by SKA is much higher than that of H I 21-cm line, the radio con-

tinuum is very suitable for the exploration of the cosmic SFR from the very early phase of galaxy formation.

By these studies, we will surely witness a real revolution in the studies of galaxies by SKA.

Acknowledgments

We are grateful to K. Kohno for useful comments. TTT has been supported by the Grant-in-Aid for the Scientific Research Fund (23340046) commissioned by the Ministry of Education, Culture, Sports, Science and Technology (MEXT) of Japan. HH thanks the support from the Ministry of Science and Technology (MoST) grant 102-2119-M-001-006-MY3.

References

Kalberla, P. M. W., & Kerp, J., 2009, ARA&A, 47, 27
Kaneko, H., et al., 2013, PASJ, 65, 20
Nakanishi, H. & Sofue, Y., 2016, PASJ, 68, 5
Nakanishi, H. et al., 2006, ApJ, 651, 804
Sofue, Y. & Rubin, V., 2001, ARA&A, 39, 137
Tosaki, T. et al., 2011, PASJ, 63, 1171
Akerman, C. J., Ellison, S. L., Pettini, M., & Steidel, C. C. 2005, A&A, 440, 499
Allen, S. W. et al. 2003, MNRAS, 342, 2887
Anders E., Grevesse N., 1989, Geochim. Cosmochim. Acta, 53, 197
Asano, R. S., Takeuchi, T. T., Hirashita, H., Nozawa, T. 2013, MNRAS, 432, 637
Asano, R. S., Takeuchi, T. T., Hirashita, H., & Nozawa, T. 2014, MNRAS, 440, 134
Babul A. & Rees M. J., 1992, MNRAS, 255, 346
Bacon R. et al., 2001, MNRAS, 326, 23
Barnes J. E. et al., 2001, MNRAS, 322, 486
Beck, S. C., Turner, J. L., Langland-Shula, L. E., Meier, D. S., Crosthwaite, L. P., & Gorjian, V. 2002, AJ, 124, 2516
Begum A. et al., 2008, MNRAS, 386, 1667
Benson A. J., et al., 2002, MNRAS, 333, 156
Bell, E. F. & de Jong, R. S., 2001, ApJ, 550, 212
Bekki, K. 2015, MNRAS, 449, 1625
Bigiel, F. et al., 2008, AJ, 136, 2846
Bigiel, F., et al., 2011, ApJ, 730, 13
Bigiel, F. & Blitz, L., 2012, ApJ, 756, 183
Black J. H., Chaffee F. H. Jr., Foltz C. B., 1987, ApJ, 317, 442
Blitz, L. & Rosolowsky, E., 2004, ApJ, 612, 29
Boselli, A. et al., 2002, A&A, 564, 66
Bosma, A., 1981, AJ, 86, 1791
Briggs F. H., Brinks E., Wolfe A. M., 1997, AJ, 113, 467
Braun R., 2012, ApJ, 749, 87
Braun R., Thilker D. A., Walterbos R. A. M., Corbelli E. 2009, ApJ, 695, 937
Buat, V., Iglesias-Páramo, J., Seibert, M., et al. 2005, ApJ, 619, L51
Buat, V., Takeuchi, T. T., Iglesias-Páramo, J., et al. 2007, ApJS, 173, 404
Butcher, H. and Oemler, Jr., A. 1978, ApJ, 219, 18
Butcher, H., Wells, D. C. and Oemler, Jr., A. 1983, ApJS, 52, 183
Cannon J. M. et al., 2011, ApJ, 739, 22
Cantinella B. et al., 2010, MNRAS, 403, 683
Catinella B. et al., 2012b, A&A, 544, 65
Catinella B. et al., 2012a, MNRAS, 420, 1959
Catinella B. et al., 2013, MNRAS, 436, 34
Cappellari M. et al., 2011, MNRAS, 416, 1680
Carilli C. L., Lane W., de Bruyn A. G., Braun R., Miley G. K., 1996, AJ, 111, 1830
Casey, C. M., et al. 2015, Next Generation Very Large Array Memos Series, No. 8 (arXiv:1510.06411)
Chapman, S. C., Blain, A. W., Smail, I., & Ivison, R. J. 2005, ApJ, 622, 772
Condon, J. J. 1992, ARA&A, 30, 575
Curran S. J., Tzanavaris P., Darling J. K., Whiting M. T., Webb J. K., Bignell C., Athreya R., Murphy M. T., 2010, MNRAS, 402, 35
Dave R., Oppenheimer B. D. & Finlator K., 2011, MNRAS, 415, 11
de Blok W. J. G. et al., 2003, MNRAS, 340, 657
de Blok W. J. G., 2005, ApJ, 634, 227
de Bruyn A. G., O'Dea C. P., Baum S. A., 1996, A&A, 305, 450
Deeg, H.-J., Brinks, E., Duric, N., Klein, U., & Skillman, E. 1993, ApJ, 410, 626
Dekel A. et al., 2009a, Nature, 457, 451
Dekel A., Sari R. & Ceverino D., 2009b, ApJ, 703, 785
Draine B. T., Bertoldi F., 1996, ApJ, 468, 269
Ellison, S. L., Hall, P. B., & Lira, P. 2005, AJ, 130, 1345
Elmegreen, B. G., 1993, ApJ, 411, 170
Fall, S. M., & Pei, Y. C. 1993, ApJ, 402, 479
Fernández, X. et al., 2013, ApJ, 770, 29
Ferrara A. & Tolstoy E., 2000, MNRAS, 313, 291
Field G. B., 1958, Proc. I.R.E., 46, 240
Fumagalli, M., Krumholz, M. R. & Hunt, L. K., 2010, ApJ, 722, 919
Fukui, Y. et al., 2015, ApJ, 798, 6
Furlanetto S. R., Oh S. P., Briggs F. H., 2006, Phys. Rep., 433, 181
Fynbo J. P. U., et al., 2011, MNRAS, 413, 2481
Garrett, M. A. 2002, A&A, 384, L19
Genzel, R., Tacconi, L. J., Combes, F., et al. 2012, ApJ, 746, 69
Giovanelli R. & Haynes M. P., 1983, AJ, 88, 881
Giovanelli R. et al., 2005, AJ, 130, 2598
Glover, S. C. O. & Mac Low, M., 2007, ApJ, 659, 1317
Glover, S. C. O. & Clark, P. C., 2012, MNRAS, 421, 9
Gnedin, N. Y., Tassis, K. & Kravtsov, A. V., 2009, ApJ, 697, 55
Gouguenheim L., 1969, A&A, 3, 281
Gould, R. J. & Salpeter, E. E., 1963, ApJ, 138, 393
Grebel E. K. et al., 2003, AJ, 125, 1926
Grossi M. et al., 2009, A&A, 498, 407
Gruppioni, C., Pozzi, F., Zamorani, G., Ciliegi, P., Lari, C., Calabrese, E., La Franca, F., Matute, I. 2003, MNRAS, 341, L1
Hibbard J. E. et al., 2001, ASPC, 240, 657
Hirashita H., Ferrara A., Wada K., Richter P., 2003, MNRAS, 341, L18 (H03)
Hirashita H., Ferrara A., 2005, MNRAS, 356, 1529

Hirashita H., & Hunt, L. K. 2006, A&A, 460, 67
Hirashita, H. 2011, MNRAS, 418, 828
Hirashita, H., et al. 2015, PASJ, submitted
Hoeft M. et al., 2006, MNRAS, 371, 401
Hollenbach D. J., McKee C. F., 1979, ApJS, 41, 555
Hollenbach, D. & Salpeter, E. E., 1971, ApJ, 163, 155
Honma, M., Sofue, Y. & Arimoto, N., 1995, A&A, 304, 1
Hunt, L. K., Dyer, K. K., & Thuan, T. X. 2005, A&A, 436, 837
Hunter D. A. et al., 2012, AJ, 144, 134
Ibar, E., et al. 2008, MNRAS, 386, 953
Inoue, A. K., Hirashita, H., & Kamaya, H. 2000, PASJ, 52, 539
Inoue, S., Omukai, K., & Ciardi, B. 2007, MNRAS, 280, 1715
Jaffe, W. J., Perola, G. C., & Tarenghi, M. 1978, ApJ, 224, 808
Jaffé, Y. L. et al. 2012, ApJ, 756, L28
Jaffé, Y. L. et al., 2013, MNRAS, 431, 2111
Jarvis, M. J., et al. 2015, in Proceednigs of Advancing Astrophysics with the Square Kilometre Array (AASKA14), 68
Johnsen, R. & Guberman, S. L., 2010, Elsevier Inc., "Advances In Atomic, Molecular, and Optical Physics", 59, 75
Kanekar N., et al., 2014, MNRAS, 438, 2131
Kanekar N., Ellison S. L., Momjian E., York B. A., Pettini M. 2013, MNRAS, 428, 532
Kanekar N., Subrahmanyan R., Ellison S. L., Lane W. M., Chengalur J. N., 2006, MNRAS, 370, L46
Kennicutt, R. C., Jr. 1998, ARA&A, 36, 189
Kennicutt, R. C., & Evans, N. J. 2012, ARA&A, 50, 531
Kennicutt, R. C., et al., 2007, ApJ, 671, 333
Klein, U., Weiland, H., & Brinks, E. 1991, A&A, 246, 323
Klein, U., Wielebinski, R., & Thuan, T. X. 1984, A&A, 141, 241
Knapp G. R. et al., 1985, AJ, 90, 454
Krumholz, M. R., McKee, C. F. & Tumlinson, J., 2008, ApJ, 689, 865
Krumholz, M. R., McKee, C. F. & Tumlinson, J., 2009, ApJ, 693, 216
Krumholz M. R., 2012, ApJ, 759, 9
Krumholz M. R., 2013, IAUS, 292, 227
Kuntschner H. et al., 2010, MNRAS, 408, 97
Kwan. J., 1977, ApJ, 216, 713
Ledoux C., Petitjean P., Srianand R., 2003, MNRAS, 346, 209
Lemonias J. J. et al., 2013, ApJ, 776, 74
Leroy, A. K. et al., 2008, AJ, 136, 2782
Levshakov S. A., Molaro P., Centurión M., D'Odorico S., Bonifacio P., Vladilo G., 2000, A&A, 361, 803
Lewis I. et al., 2002, MNRAS, 334, 673
Liszt, H., 2002, A&A, 389, 393
London. R., McCray. R. & Chu, S.-I., 1977, ApJ, 217, 442
Mac Low M. & Ferrara A., 1999, ApJ, 513, 142
Mac Low, M. & Glover, S. C. O., 2012, ApJ, 746, 135
Magnelli, B., Saintonge, A., Lutz, D., et al. 2012, A&A, 548, AA22
Magnelli, B., Lutz, D., Saintonge, A., et al. 2014, A&A, 561, AA86
Magorrian, J., Tremaine, S., Richstone, D., et al. 1998, AJ, 115, 2285
Martin A. M. et al., 2010, ApJ, 723, 1359
McGaugh S. S. et al., 2000, ApJ, 533, 99
McGaugh S. S., 2005, ApJ, 632, 859
McGaugh, S. S., 2012, AJ, 143, 40
McKee, C. F. & Krumholz, M. R., 2010, ApJ, 709, 308
Michałowski, M. J., Watson, D., & Hjorth, J. 2010, ApJ, 712, 942
Momose, R., Koda, J., Kennicutt, R. C., Jr., et al. 2013, ApJ, 772, LL13
Moran S. M. et al., 2012, ApJ, 745, 66
Morganti R. et al., 2006, MNRAS, 371, 157
Morganti, R., Sadler, E. M., & Curran, S. 2015, in Proceednigs of Advancing Astrophysics with the Square Kilometre Array (AASKA14), 134
Mori M., Ferrara A. & Madau P., 2002, ApJ, 571, 40
Mori M. & Umemura M., 2006, Nature, 440, 644
Morrison, G. E., Owen, F. N., Dickinson, M., Ivison, R. J., & Ibar, E. 2010, ApJS, 188, 178
Murphy, E. J. 2009, ApJ, 706, 482
Murphy, E. J., et al. 2015, in Proceednigs of Advancing Astrophysics with the Square Kilometre Array (AASKA14), 85
Navarro J. F. et al., 2004, MNRAS, 349, 1039
Neufeld, D. A. & Spaans, M., 1996, ApJ, 473, 894
Okamoto, T. 2013, MNRAS, 428, 718
Omukai K., 2000, ApJ, 534, 809
Omukai, K., et al., 2010, ApJ, 722, 1793
Oosterloo T. et al., 2010, MNRAS, 409, 500
Ott J. et al., 2012, AJ, 144, 123
Pelupessy, F. I., Papadopoulos, P. P. & van der Werf, P., 2006, ApJ, 645, 1024
Péroux C, McMahon R. G., Storrie-Lombondi L. L., Irwin M. J., 2003, MNRAS, 346, 1003
Petitjean P., Ledoux C., Noterdaeme P., Srianand R., 2006, A&A, 456, L9
Petitjean P., Srianand R., Ledoux C., 2000, A&A, 364, L26
Pisano, D. J., 2014, AJ, 147, 48
Prandoni, I., & Seymour, N. 2015, in Proceednigs of Advancing Astrophysics with the Square Kilometre Array (AASKA14), 67
Prochaska J. X., Wolfe A. M., 2002, A&A, 566, 68
Razoumov, A. O., Norman, M., Prochaska, J. X., & Wolfe, A. M. 2006, ApJ, 645, 5
Rees M. J., 1986, MNRAS, 218, 25
Richings, A. J., Schaye, J. & Oppenheimer, B. D., 2014, MNRAS, 442, 2780
Roberts, M. S., & Haynes, M. P. 1994, ARA&A, 32, 115
Roussel, H., Helou, G., Beck, R., Condon, J. J., Bosma, A., Matthews, K., & Jarrett, T. H. 2003, ApJ, 593, 733
Rowlands, K., et al. 2014, MNRAS, 441, 1017
Rubin, V. C., Thonnard, N. & Ford, W. K. Jr., 1980, ApJ, 238, 471
Rubin, V. C. et al., 1985, ApJ, 289, 81
Sargent, W. L. W., Young, P. J., Boksenberg, A., & Tytler, D. 1980, ApJS, 42, 41
Saitoh, T. R., Daisaka, H., Kokubo, E., Makino, J., Okamoto, T., Tomisaka, K., Wada, K., & Yoshida, N. 2009, PASJ, 61, 481
Sancisi, R., 1983, IAU symposium, 100, 55
Sancisi, R. & van Albada, T. S., 1987, IAU symposium, 117, 67

Sancisi, R. & van Albada, T. S., 1987, "Dark matter" IAU symposium, 124, 699
Sandage A. et al., 1970, ApJ, 160, 831
Scannapieco E., Silk J. & Bouwens R., 2005, ApJ, 635, 13
Schiminovich, D., Wyder, T. K., Martin, D. C., et al. 2007, ApJS, 173, 315
Scoville, N., et al. 2007, ApJS, 172, 1
di Serego Alighieri S. et al., 2007, A&A, 474, 851
Seymour, N., et al. 2008, MNRAS, 386, 1695
Serra P. et al., 2012, MNRAS, 422, 1835
Schiminovich D. et al., 2010, MNRAS, 408, 919
Smith, H. E., Cohen, R. D., & Bradley, S. E. 1986, ApJ, 310, 583
Smolčić, V., et al. 2014, MNRAS, 443, 2590
Smolčić, V., et al. 2009, ApJ, 690, 610
Sofue, Y., Honma, M. & Arimoto, N., 1995, A&A, 296, 33
Spitzer L. Jr. & Baade W., 1951, ApJ, 113, 413
Srianand, R., Gupta, N., Petitjean, P., Noterdaeme, P., Ledoux, C., Salter, C. J., & Saikia, D. J. 2012, MNRAS, 421, 651
Sternberg, A., 1988, ApJ, 332, 400
Struve, C., & Conway, J. E. 2012, A&A, 546, 22
Symeonidis, M., Vaccari, M., Berta, S., et al. 2013, MNRAS, 431, 2317
Takahashi, J., Masuda, K. & Nagaoka, M., 1999, MNRAS, 306, 22
Takahashi, J. 2000, Astronomical Herald, 93, 191
Takeuchi, T. T., Kawabe, R., Kohno, K., Nakanishi, K., Ishii, T. T., Hirashita, H., & Yoshikawa, K. 2001, PASP, 113, 783
Tanaka, A. et al., 2014, PASJ, 66, 66
Teruya, N. & Takeuchi, T. T., 2014, in "The Impact of Galactic Structure on Star Formation", Sapporo, Japan
Thomas D. et al., 2010, MNRAS, 404, 1775
Tinsley, B. M. 1980, Fundam. Cosm. Phys., 5, 287
Tinsley, B. M., & Danly, L. 1980, ApJ, 242, 435
Totani, T., & Takeuchi, T. T. 2002, ApJ, 570, 470
Tully, R. B. & Fisher, J. R., 1977, A&A, 54, 661
van den Bergh S., 1976, ApJ, 206, 883
van den Bosch F. C. & Swaters R. A., 2001, MNRAS, 325, 1017
van Dishoeck, E. F. & Black, J. H., 1986, ApJS, 62, 109
van Gorkom J. & Schiminovich D., 1997, ASPC, 116, 310
Vanzi, L., Cresci, G., Telles, E., & Melnick, J. 2008, A&A, 486, 393
Verheijen, M. et al., 2007, ApJ, 668, 9
Vladilo G., Péroux C. 2005, A&A 444, 461
Voges, W. et al. 1999, ApJ, 756, L28
Wada K., Norman C. A., 2001, ApJ, 546, 172
Walter, F. et al., 2008, AJ, 136, 2563
Wang J. et al., 2011, MNRAS, 412, 1081
Wardle M. & Knapp G. R., 1986, AJ, 91, 23
Weldrake D. T. F. et al., 2003, MNRAS, 340, 12
Wolfe, A. M., & Davis M. M. 1979, AJ, 84, 699
Wolfe A. M., Briggs F. H., Turnshek D. A., Davis M. M., Smith H. E., Cohen R. D. 1985, ApJ, 294, L67
Wolfe, A. M., Turnshek, D. A., Smith, H. E., & Cohen, R. D. 1986, ApJS, 61, 249
Wolfe, S. A. et al., 2013, Nature, 497, 224
Wong, T. & Blitz, L., 2002, ApJ, 569, 157
Wong, T. et al., 2013, ApJ, 777, 4
Yajima, H., Shlosman, I., Romano-Díaz, E., & Nagamine, K. 2015, MNRAS, 451, 418
York D. G. et al., 2000, AJ, 120, 1579
Yoshida N. et al., 2006, ApJ, 652, 2
Yoshida N. et al., 2008, Science, 321, 669
Yun, M. S., Reddy, N. A., & Condon, J. J. 2001, ApJ, 554, 803
Zaritsky, D. et al., 2014, AJ, 147, 134